NUREG/GR-0004

Measurement and Modeling of Sensitization Development in Stainless Steels as a Function of Thermomechanical Processing

Prepared by
D. G. Atteridge, S. M. Bruemmer, J. W. Simmons, M. Li

Department of Materials Science and Engineering
Oregon Graduate Institute of Science and Technology

Prepared for
U.S. Nuclear Regulatory Commission

9212140232 921130
PDR NUREG
GR-0004 R PDR

NOTICE

This document was prepared with the support of the U.S. Nuclear Regulatory Commission (NRC) Grant Program. The purpose of the NRC Grant Program is to support basic, advanced, and developmental scientific research for a public purpose in areas relating to nuclear safety. The nature of NRC's Grant Program is such that the grantee bears prime responsibility for the conduct of the research and exercises judgement and original thought toward attaining the scientific goals. The opinions, findings, conclusions and recommendations expressed herein are therefore those of the author(s) and do not necessarily reflect the views of the NRC.

Available from

Superintendent of Documents
U.S. Government Printing Office
P.O. Box 37082
Washington, DC 20013-7082

and

National Technical Information Service
Springfield, VA 22161

NUREG/GR–0004
R5

Measurement and Modeling of Sensitization Development in Stainless Steels as a Function of Thermomechanical Processing

Manuscript Completed: October 1992
Date Published: November 1992

Prepared by
D. G. Atteridge, S. M. Bruemmer*, J. W. Simmons, M. Li

Department of Materials Science and Engineering
Oregon Graduate Institute of Science and Technology
Beaverton, OR 97006–1999

Prepared for
Division of Engineering
Office of Nuclear Regulatory Research
U.S. Nuclear Regulatory Commission
Washington, DC 20555
NRC FIN G1107
Under Grant No. NRC–G–04–87–105

*Pacific Northwest Laboratory
Richland, WA 99352

ABSTRACT

An analytical model has been developed for predicting thermomechanical effects on the development of grain boundary chromium depletion in austenitic stainless steel as a first step in predicting intergranular stress corrosion cracking susceptibility. Model development and validation is based on sensitization development analysis of over 30 Type 316 and 304 stainless steel heats. The data base included analysis of deformation effects on resultant sensitization development. Continuous cooling sensitization behavior is examined and modeled with and without strain. Gas tungsten arc girth pipe weldments are also characterized by experimental measurements of heat affected zone temperatures, strains and sensitization during/after each pass; pass by pass thermal histories are also predicted. The model is then used to assess pipe chemistry changes on chromium depletion changes.

CONTENTS

FIGURES

TABLES

1.0 INTRODUCTION

It has long been known that intergranular stress corrosion cracking (IGSCC) of austenitic Type 300 Series stainless steels (SS) is directly related to the presence of grain boundary chromium depletion, and that this depletion, also called "sensitization", is caused by the formation of grain boundary chromium carbides/nitrides.[1] Thus it is well documented that susceptibility to IGSCC is caused by a diffusion controlled process. However, quantification of this phenomenon is still an active research area, and the research reported herein pertains to the development of a computer-based model capable of predicting sensitization development (and thus, indirectly, IGSCC susceptibility) in mill annealed (MA) and solution annealed (SA) type 304 and 316 SS. The specific thermomechanical processing assessed under this program was the effect of strain on sensitization developed during linear cooling as a function of peak temperature and cooling rate. Subsequent model predictions of sensitization development in the heat affected zone (HAZ) of Type 304 and 316 SS girth pipe weldments are also discussed.

Programmatic work has covered a time frame of several years and has consisted of development of a sensitization prediction model and a data base to validate and/or dictate further model development. The work reported herein is limited to second generation model development and the data base which drove recent model development. Validation data base development as well as programmatic model development was initiated by Bruemmer.[2-4] Subsequent linear continuous cooling (CC) data validation experimentation was done by Simmons and Cedeño.[5,6] Work reported herein is limited to the linear CC data base developed by Simmons and the subsequent CC model development done by Li.

Model predictions are based on prediction of chromium depletion at grain boundaries. It is assumed that as grain boundary sensitization increases susceptibility to IGSCC increases. A demonstration of this relationship determined by constant extension rate (CERT) testing is presented in Figure 1.[2] Note that "EPR-DOS" is a measurement of degree of sensitization (DOS) determined by the electrochemical potentiokinetic reactivation (EPR) test, as discussed in the Sensitization Measurement Section below. The model predicts levels of sensitization, with susceptibility to IGSCC estimated on a system by system assessment.

The model, SSDOS, originally developed by Bruemmer, assesses the effect of both thermodynamics and kinetics on the development of sensitization, as illustrated in Figure 2.[2,3] Thermodynamics are needed to assess chromium minimums at the matrix-carbide interface as a function of SS composition and diffusion temperature, see Figure 3.[2,3] These matrix-carbide "equilibrium" chromium concentrations are assumed to control, and indeed be equal to, grain boundary chromium concentrations. Bruemmer assumed this was a valid first approximation due to increased grain boundary diffusivity, in comparison to matrix diffusivity. The chromium minimum is then used in diffusion calculations in developing chromium depletion grain boundary profiles as a function of temperature and time.

Original model concepts assumed instantaneous attainment of equilibrium chromium minimum values and allowed sensitization to develop as a function of temperature and time.[2-4] Modifications to the SSDOS isothermal section by Bruemmer and Advani incorporated a nucleation time incubation period prior to initiation of diffusional growth of the chromium depletion zone.[2,3,8] Research into sensitization development induced by CC also indicates that inclusion of nucleation

times is critical for realistic predictions of sensitization development.[6,8] Both isothermal and CC research work has shown that plastic strain dramatically increases sensitization development.[2-4, 6-8] Work reported herein discusses programmatic developments in modeling CC experimental results and application of these techniques to prediction of weld induced sensitization.

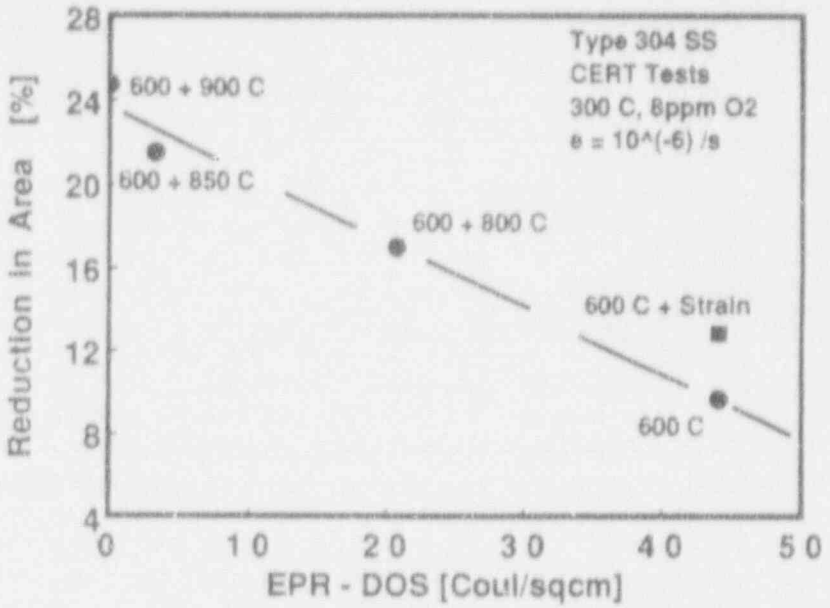

Figure 1. Correlation Between Degree of Sensitization as Measured by EPR and Ductility as Measure in Slow-Strain-Rate Stress Corrosion Cracking Tests.

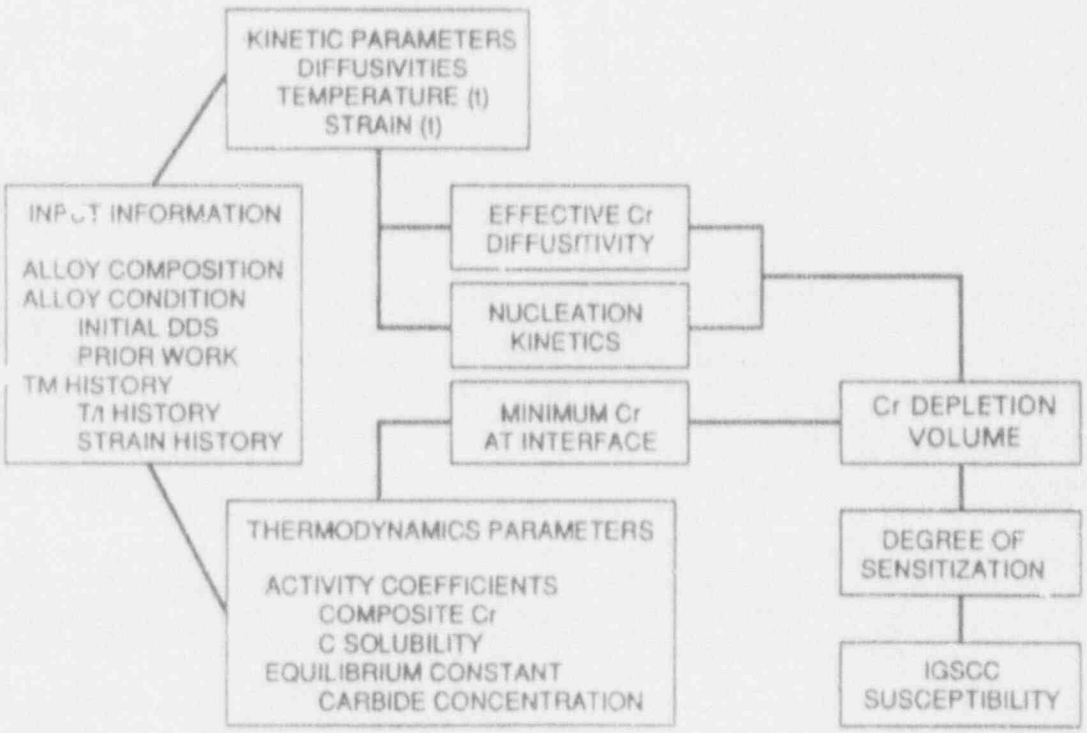

Figure 2. Flow Diagram Illustrating Degree of Sensitization Prediction Approach.

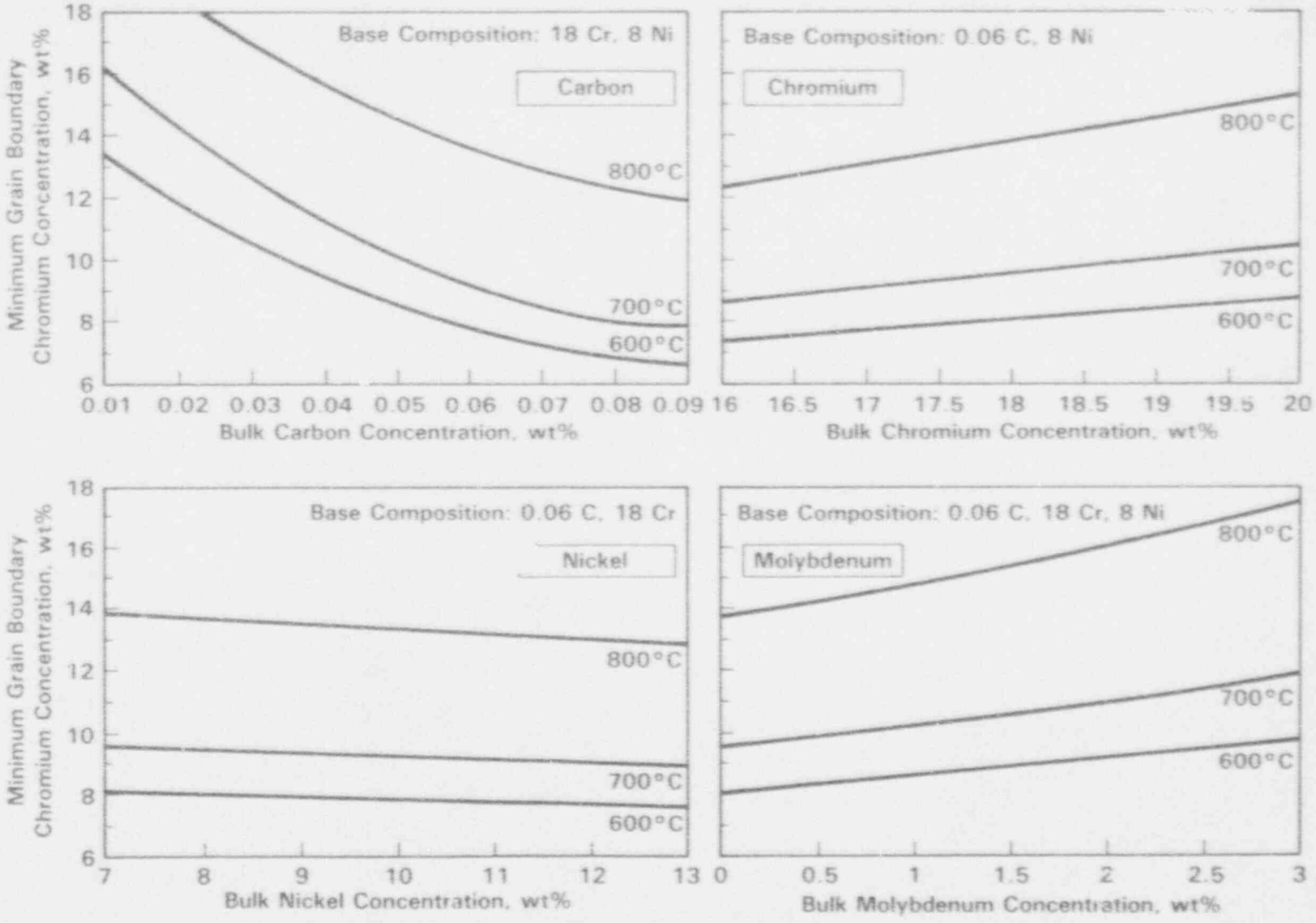

Figure 3. Model Predictions Illustrating Bulk Composition Effects on Sensitization.

2.0 EXPERIMENTAL PROCEDURES

2.1 Materials

The materials used to assess linear cooling model validation were high carbon 316 austenitic SSs, received in the form of 10cm (4-inch) diameter pipe (Schedule 40) in the MA condition (final anneal at 1100°C for 5 minutes).[2,5-7] The bulk composition of the material (expressed in weight percent) for Alloy 16 was nominally 0.058 C, 17.1 Cr, 11.4 Ni, 2.3 Mo, 0.41 Si, 0.014 P, and 0.008 N while Alloy 17 was nominally 0.067 C, 16.8 Cr, 11.2 Ni, 2.2 Mo, 0.28 Si, 0.016 P, and 0.071 N. Alloy 16 MA material had a uniform equiaxed grain structure with an average grain diameter of 95 microns while Alloy 17 had an average grain diameter of 60 microns. The majority of the experimental matrix utilized material in the MA condition for a variety of reasons. First, virtually all pipes used in (nuclear) industry are welded in the MA condition, and, second, results of transmission electron microscopy (TEM) showed that the initial MA material did not contain any detectable carbides and that the material in MA and solution annealed (SA) conditions (1100°C for 1 hour) had equal dislocation densities. Finally, EPR testing of the MA material substantiated that it was not sensitized.

2.2 Material Deformation and Thermal Cycling

The test specimens were sectioned from the as-received pipe in the longitudinal direction and were 13cm (5 inches) in length, 1.25cm (0.5 inches) wide, and 0.65cm (0.25 inches) thick (equal to the pipe thickness). Mill annealed and SA specimens from both alloys were subjected to CC thermal cycles. Prior deformation of selected Alloy 17 MA specimens was performed at ambient temperature in uniaxial tension and subsequently subjected to CC thermal cycles. Three levels of prior strain (5%, 10%, and 20%) were used (calculated as true-strain by reduction-of-area measurements). The strain levels obtained in all of the specimens were within +/- 1% (absolute percentage of strain) of the nominal values.

Continuous cooling thermal cycling of all specimens used for model validation was performed in a computer-controlled Gleeble thermal simulator. In a Gleeble, the specimen to be cycled is generally held between two water-cooled copper grips and directly heated by passing a low-frequency alternating current through it. Stainless steel jaws were used in the Gleeble, in the present work, to reduce heat conduction through the grips and resulted in a constant temperature zone of approximately 1.25 cm (0.5 inches) at specimen mid-span.[5-7] The feedback signal necessary for closed loop control of the current and accurate temperature control was obtained from a fine wire K-type (chromel-alumel) thermocouple welded to the specimen at mid-span.

Thermal cycles utilized in the current work can be divided into four specific segments: (1) linear heating region; (2) peak cycle temperature; (3) linear cooling region; and (4) minimum temperature reached during cooling, prior to air quenching. Typical test specimens were heated linearly at a rate of 50°C/sec, subjected to peak temperatures ranging from 800 to 1050°C,

continuously cooled to 400°C using three linear cooling rates of 0.05, 0.10, and 1.0°C/sec, and then air cooled to room temperature. The cooling cycle was initiated immediately upon reaching the peak temperature. A typical CC thermal cycle used in the study is shown in Figure 4.

A series of samples were subjected to CC thermal cycles as described above except that they were quenched in a stream of compressed air from various cycle temperatures within the sensitization regime (i.e., above 400°C) in order to gain a better understanding of DOS development during cooling.[6,7] This allowed evaluation of EPR-DOS development during cooling to be characterized as a function of temperature (and time) during individual linear CC instead of only assessing effectiveness of the total cycle on sensitization development.

2.3 Degree of Sensitization Measurements

The DOS of each test specimen was measured using the single loop EPR test, as proposed by Clarke.[9-10] The EPR test was repeated on each sample 3 times and the results averaged to determine the EPR-DOS. The single loop EPR test method consists of developing potentiokinetic curves of a polarized specimen by the use of a controlled potential sweep from the passive region to the active region (reactivation). A passive film is first formed on the specimen surface and then break-down of this film is characterized by the severity of grain boundary attack that occurs in the Cr-depleted regions during reactivation. Non-sensitized SSs exhibit a low current density during the reactivation step resulting from the stability of the passive film. However, sensitized SSs show higher current densities due to passive film breakdown in Cr-depleted regions near grain boundaries.[9-13]

The parameters of the EPR test are listed in Table I. The EPR tests were performed according to the following procedure: (1) the open-circuit corrosion potential (E_c) of the working electrode versus SCE was measured; (2) the sample was passivated at a passivation potential (E_p) of +200 mv for 2 minutes; (3) the reactivation scan was performed by sweeping the potential of the sample from the E_p to E_c at a rate of 3 volts/hour; (4) the area of the reactivation peak was integrated during the reactivation scan to obtain the total charge value, Q. The integral charge value, Q, was subsequently normalized to the grain boundary area (GBA) of each test specimen to obtain the normalized total charge Pa (EPR-DOS) value (coul./cm^2), using the relationship outlined by Clarke et al.:[9]

$$Pa\ (coul./cm^2) = Q/(GBA) \quad (1)$$

$$GBA = As[5.1 \times 10^{-3} \exp(0.35X)] \quad (2)$$

where (As) is the masked specimen area (cm^2) and (X) is the ASTM grain size at a magnification of 100. The grain size of specimens from each sample set were measured using the three-circle method outlined in ASTM E112 after electrolytic etching with an aqueous solution of 60% nitric acid. An illustration of increasing EPR-DOS with increasing corrosion current flow from previously passivated specimen surfaces is shown in Figure 5.

Specimens were metallographically examined after EPR testing since prior deformation has been reported to induce transgranular (TG) carbide precipitation in austenitic SSs. Transgranular precipitation of carbides inhibits quantification of the EPR test (since the results are normalized to

grain boundary area where all of the attack is assumed to take place) and may have an influence on the grain boundary chromium-depletion profiles. Transgranular precipitation has also been reported to decrease the susceptibility of sensitized austenitic materials to IGSCC.[13 15]

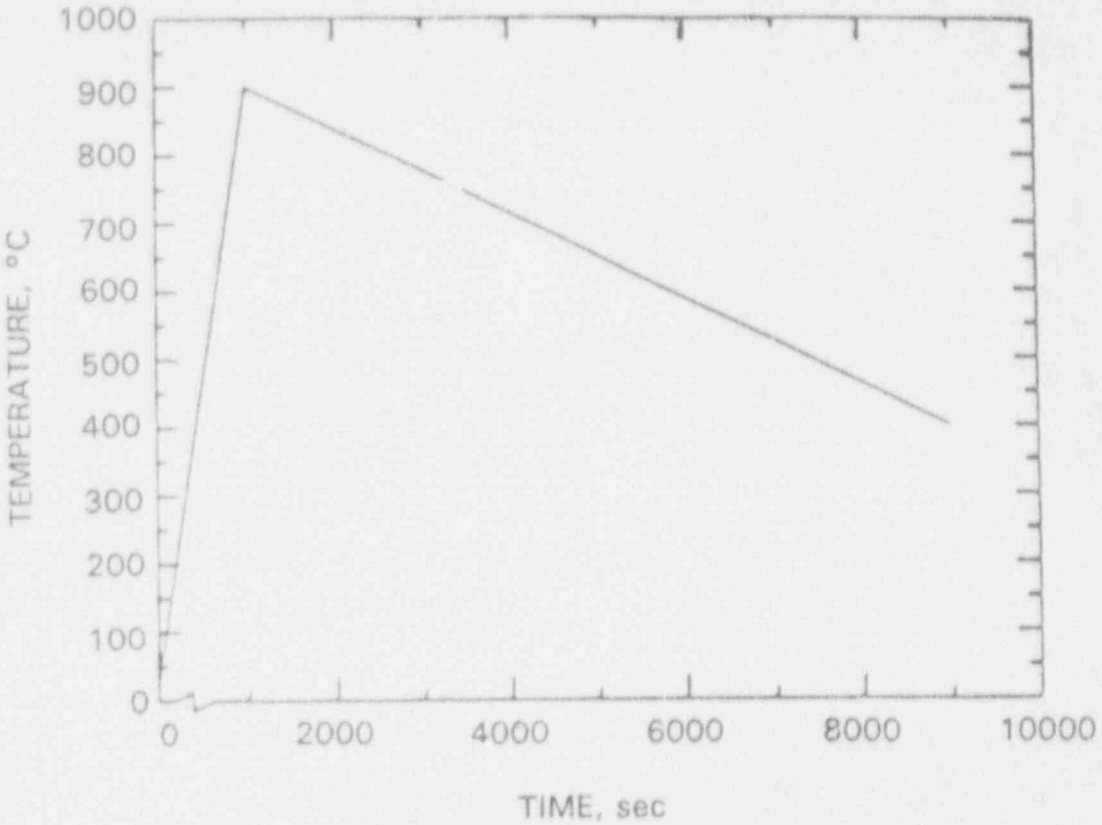

Figure 4. Typical Continuous Cooling Gleeble Thermal Cycle Illustrating Maximum Temperature and Linear Cooling Rate.

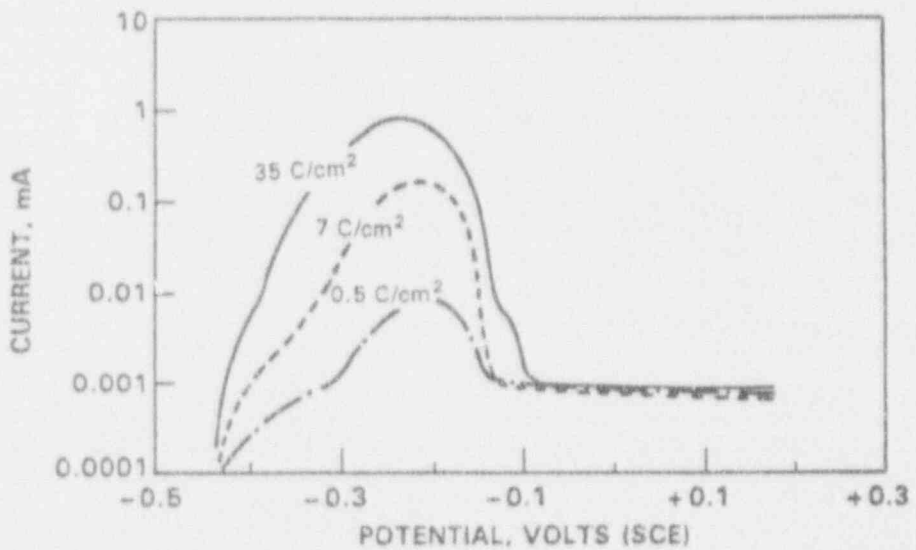

Figure 5. Examples of Potentiokinetic Reactivation measurements for Different Levels of Sensitization, EPR-DOS Values are Indicated.

3.0 RESULTS AND ANALYSIS

The results and analysis section is broken down into two main headings; one for presentation of results from Alloy 17 MA experimental studies and the other for presentation of results from sensitization modeling studies. The continuous cooling experimental results presented herein and subsequently used for model development and validation are restricted to Simmons' gleeble study results, as these represent the most quantitative test results obtained under this study.[6,7]

Presentation of the experimental studies will initially present the CC sensitization results for Alloy 17 MA material; presentation of MA prestrain study results on Alloy 17 will follow. No prestrain testing was done using Alloy 16 and its generic MA response was similar to that of Alloy 17; this is also true for SA Alloy 16 and 17. Thus these experimental results are not presented in this section. The various absolute EPR-DOS differences found between the various Alloys and solution annealing heat treatment responses are important to modeling considerations and, therefore, are discussed in that section.

3.1 MA Sensitization Induced by Continuous Cooling Alloy 17

Continuous cooling sensitization development of Alloy 17 MA material as a function of peak temperature and cooling rate is illustrated in Figure 6. Sensitization development was observed to be a strong function of the peak temperature reached during the thermal cycle. For the particular heat of material studied, CC from peak temperatures above 950°C resulted in a dramatic decrease in EPR-DOS.

The peak cycle temperature which produced the highest experimentally determined DOS during CC sensitization was defined as the critical peak temperature. Thermal cycles with peak temperatures below the critical peak temperature produced decreasing EPR-DOS values with decreasing peak temperatures. From the data shown in Figure 6, it appears as though the critical peak temperature varies as a function of cooling rate. However, as it is likely that the actual critical peak temperature for CC sensitization of this material falls between 900 and 950°C, it is also possible for all cooling rates to have the same critical peak temperature somewhere between 900 and 950°C. Data was not sufficient to differentiate between these two hypothesis. For all peak temperatures, DOS increased with decreasing cooling rate. Of course, this trend was expected since the amount of time spent in the sensitization range increases with decreasing cooling rates.

The general trends of the current CC sensitization results correlate well with those reported by other investigators, most notably those of Solomon and Bruemmer.[2,17,18] The presence of a critical peak temperature, for which sensitization development is most rapid, was also observed by Solomon and Bruemmer. Solomon suggested that the critical peak temperature occurs just below the (predicted) carbide solubility temperature for a given material.[19] Although no direct evidence

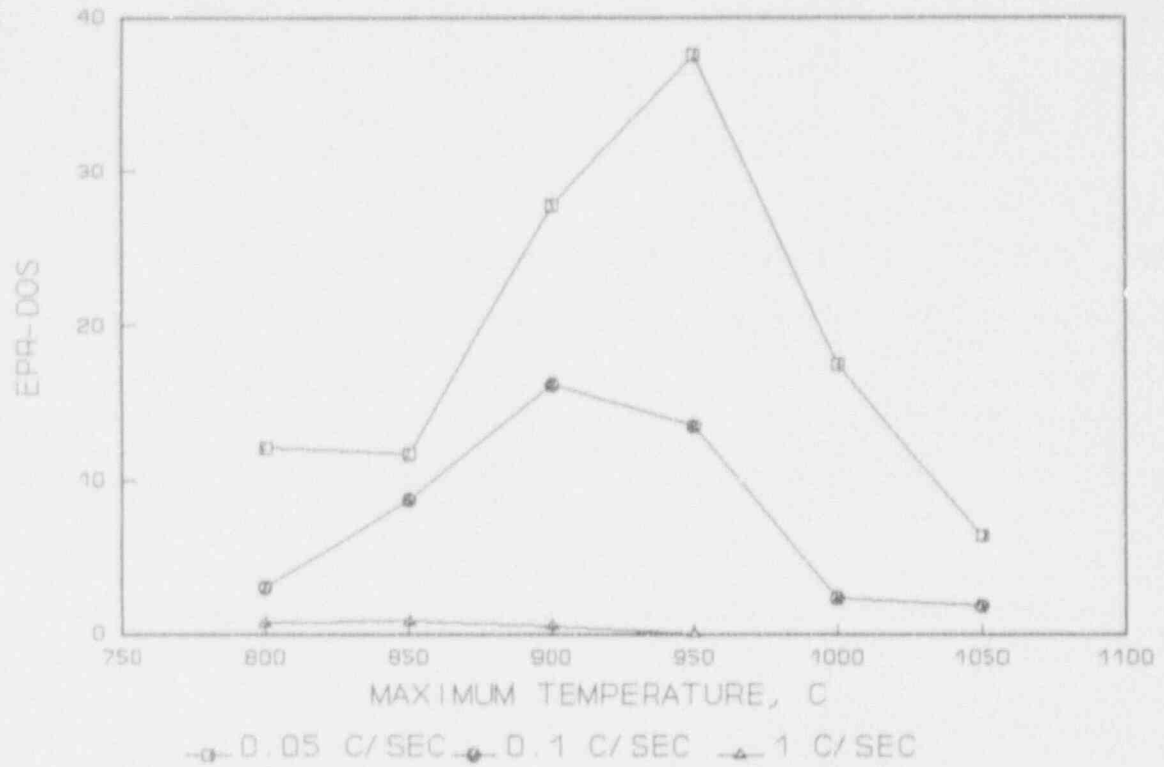

Figure 6. Measured EPR-DOS Values for Mill Annealed Alloy 17 Material as a Function of Peak Temperature and Cooling Rate.

has been presented, it seems logical that the critical peak temperature effect is associated with the carbide solubility temperature, and this concept was used in programmatic model development, as discussed below. If this is true, it is to be expected that any carbides present would be dissolved thus making renucleation of the carbides much more difficult upon subsequent cooling when the temperature reached during the continuous cooling cycle is above the critical peak temperature.[19]

The critical peak temperature for sensitization of alloy 17 material in the current work was defined as being between 900 and 950°C, probably closer to 950°C, and the carbide solubility temperature for the material used in this study was calculated to be approximately 980°C. Carbon solubility in Type 316 SS as a function of temperature was calculated from the work of Deighton[20] and is illustrated in Figure 7.

3.2 Sensitization Induced in Alloy 17 During the Cooling Cycle

In the current work, sensitization development during the cooling cycle was measured as a function of minimum cycle temperature. The sensitization response of Alloy 17 material, as a function of the minimum temperature reached during the cooling cycle, prior to quenching, is

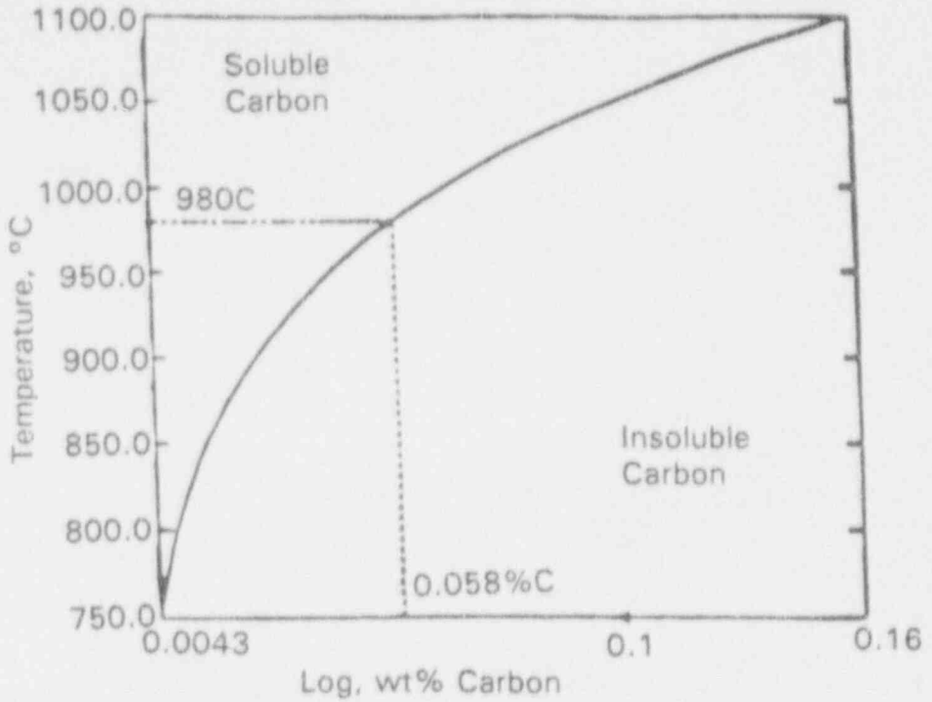

Figure 7. Variation of Carbon Solubility for Type 316 Stainless Steel as a Function of Temperature and Carbon Content.[7]

illustrated in Figure 8. It should be remembered that the samples for this study were cycled in a manner similar to previous samples except that they were quenched during the cooling cycle from temperatures above 400°C. Specifically, the samples were heated to a peak cycle temperature and cooled through the sensitization temperature regime at a specific rate, but, instead of being cooled all the way down to 400°C, were quenched prior to 400°C being reached so that DOS development could be studied as a function of minimum cycle temperature. Sensitization development for peak cycle temperatures of 850, 950 and 1050°C is shown in Figure 8.

The results obtained present direct evidence that high temperature exposures, above the critical peak temperature (specifically 1050°C), significantly retard sensitization development upon subsequent slow cooling through the primary sensitization temperature regime. The most likely explanation for this is that retardation of carbide nucleation occurred as a result of heating above the carbide solubility temperature for the particular material. This conclusion is reasonable since the onset of sensitization in materials heated to 1050°C occurred between 800 and 750°C, while for a peak temperature of 950°C, sensitization was measured in specimens quenched from as high as 900°C. Ikawa et al.,[21] demonstrated that heating 304 SS samples initially to 1100°C for two-minutes prior to isothermal annealing at temperatures between about 650 and 900°C (without returning to room temperature), resulted in a shift of the C-curve for $M_{23}C_6$ precipitation to longer times as compared to samples heated directly from room temperature to the aging temperature (Figure 9). The current results and conclusions are supported by Ikawa's findings.

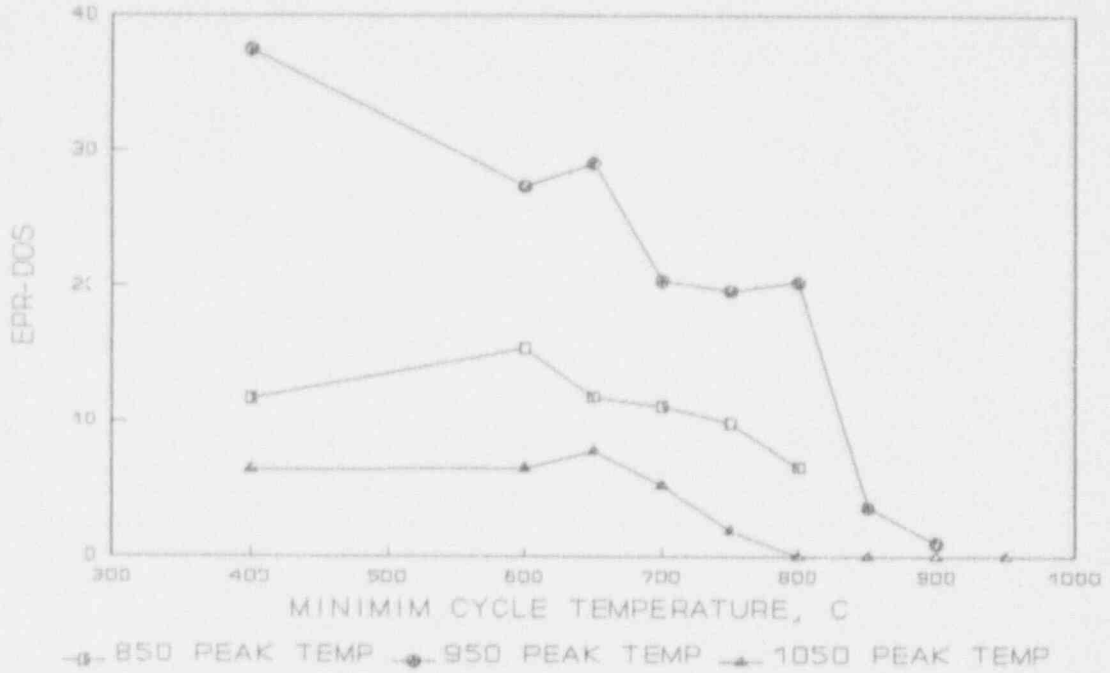

Figure 8. Measured Sensitization Development During Linear Cooling from Peak Temperatures for Mill Annealed Alloy 17 Material as a Function of Peak Temperature at a Cooling Rate of 0.05°C/sec.

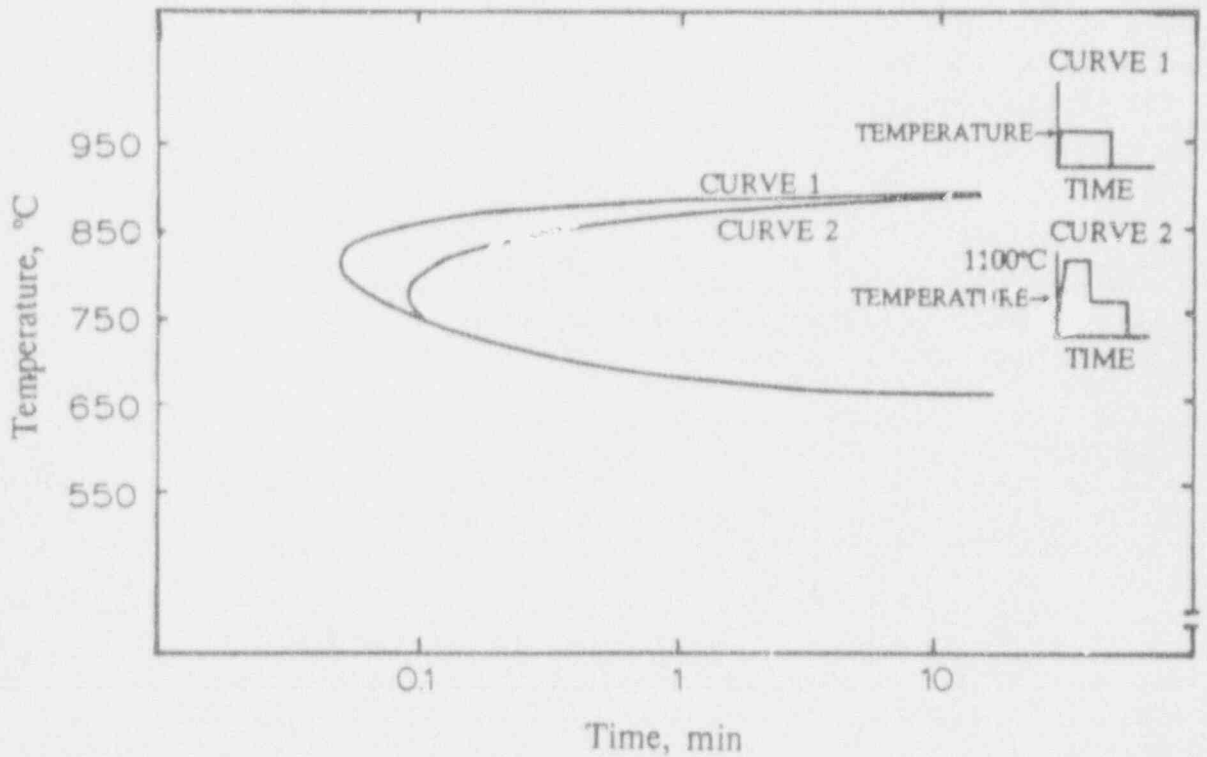

Figure 9. Change of $M_{23}C_6$ Precipitation Kinetics due to Pre-Isothermal Hold Temperature for a 0.05% Type 304 [After Ikawa et al[21]].

In the critical evaluation of this type of data, it should be remembered that the chromium content in thermodynamic equilibrium with the carbides (frequently referred to as the minimum chromium content at the grain boundaries) increases with increasing temperature, Figure 3. This is expected to result in lower EPR-DOS values being measured for given Cr-depletion widths for samples quenched from temperatures greater than 408°C as compared with samples slow cooled all the way down to 400°C, which would be expected to have lower grain boundary Cr-minimums, and thus complicate data interpretation. In the current work this is not considered to be a major factor since Bruemmer[13] correlated experimentally measured grain boundary Cr-depletion (width and minimum) to EPR-DOS data and determined that, although the grain boundary Cr-minimum has an effect on EPR-DOS values, depletion width controls its magnitude in most cases.

The data of Figure 8 shows that virtually all of the sensitization development in samples heated to a peak temperature of 850°C occurred by the time the sample was slow cooled (0.05°C/sec) to a temperature of about 700°C. About half of the total sensitization value had already developed during slow cooling between the peak cycle temperature of 850°C and a temperature of 800°C. Short nucleation times and rapid carbide growth rates are characteristic of temperatures between 850 and 800°C. The 950°C peak temperature results also indicate approximately half the final EPR-DOS attained by 800°C. Yet the 1050°C peak temperature results indicate no sensitization until below 800°C. Thus it appears that the material subjected to a peak temperature of 1050°C passed through the most active sensitization development regime during cooling prior to carbide nucleation.

For a peak cycle temperature of 1050°C and a cooling rate of 0.05°C/sec, most of the sensitization development appears to have occurred by the time the sample was slow cooled to a temperature of about 700°C. However, for a peak temperature of 1050°C, no sensitization values were measured for samples slow cooled to minimum temperatures down to 800°C. This is in stark contrast to the 850 and 950°C peak temperature results where sensitization development occurred immediately upon cooling from the peak temperature. For the 950°C peak temperature (Figure 8), EPR-DOS values (greater than zero C/cm^2) were measured in samples quenched from 900°C, indicating sensitization development above 900°C.

Only about 25% of the total sensitization value (DOS value of a sample cooled all the way to 400°C) had developed during slow cooling between the peak cycle temperature of 1050°C and a temperature of 750°C compared to 66% for the 850 and 950°C peak temperatures. Also, as shown earlier in Figure 6, total DOS development for samples heated to a peak temperature of 1050°C was equal to or less than one quarter of the DOS development in samples heated to a lower peak temperature of 950°C. Yet it is clear that samples heated to 1050°C spent at least as much time in the sensitization regime as those heated to 950°C. Thus time spent in the sensitization region does not, by itself, control subsequent sensitization development.

3.3 Effects of Prior Deformation on Continuous Cooling Sensitization in Alloy 17

The effects of prior deformation on CC sensitization development in Alloy 17 are presented in Figure 10 as a function of peak temperature, prior deformation and cooling rate. Three-dimensional (3-D) representations of this data is presented in Figures 11, 12, and 13 for cooling rates of 1.0, 0.10, and 0.05°C/sec, respectively. The 3-D surface grids were constructed by plotting experimentally determined EPR-DOS data as a function of peak cycle temperature and prior strain.

In certain regions of the plots, such as between 10 and 20% prior strain, data extrapolation was utilized so that uniform surface grids could be obtained. Three-dimensional observation of this type allows sensitization for this particular alloy to be mapped for prior deformation from 0 to 20%, peak cycle temperatures from 800 to 1050°C, and cooling rates from 0.05 to 1.0°C/s.

It is clear from the 3-D surface plots that prior deformation significantly enhanced the rate of CC sensitization development in the 316 SS used in the present study. Significant enhancement of sensitization development occurred with as little as 5% strain and DOS continued to increase with increasing strain up to the strain limit of 20% used in this study. This trend is especially clear for peak cycle temperatures below 950°C. However, deviations from this general trend are evident when the EPR-DOS values for 10 and 20% prior strain samples are compared for a cooling rate of 0.05°C/s (Figure 13). These differences can be explained on the basis of strain recovery for the higher peak cycle temperatures as detailed below.

As expected, prestrained specimens showed the same effects of peak temperature (critical peak temperature phenomenon) as the MA material. As shown in Figures 11-13, the peak temperature observed was not constant for all cycles, but was either 900°C or 950°C. The critical peak temperature (~ 950°C) was generally the same for the MA and 5% prior strain specimens at all cooling rates. For a cooling rate of 1.0°C/sec, all MA and prior strain specimens had a critical peak temperature of 950°C. However, for a cooling rate of 0.10°C/sec, the 10% and 20% prior strain specimens showed almost equal EPR-DOS values at a peak temperature of 900°C as for a peak temperature of 950°C. Finally, at a cooling rate of 0.05°C/sec, the 10% and 20% prior strain specimens showed a definite decrease in the critical peak temperature as EPR DOS values were significantly higher for a peak temperature of 900°C than for 950°C.

Limited TG carbide precipitation was observed in 20% prior strain samples heated to peak temperatures of 800, 850, and 900°C (cooling rates of 0.05°C/sec and 0.10°C/sec). However, TG precipitation was not evident in the 20% prior strain specimens heated to a peak temperature of 950°C. It should be noted that recrystallization did not occur in any of the samples during this study. Therefore, it can be concluded from the EPR test data and microstructural analyses that strain recovery played an important role in the current work. Recovery was especially significant in 10% and 20% prior strain samples heated to peak temperatures of 950°C and above.

These results are very significant in that, although the 10 and 20% prior strain samples showed evidence of recovery at 950°C, the DOS in these specimens was still significantly higher than the MA samples. The prior strain samples also had higher EPR-DOS values than the MA material at a peak temperature of 1000°C where the rate of strain recovery is greater than at 950°C. Interestingly, even the 10 and 20% prior strain samples showed enhanced EPR-DOS for a peak cycle temperature of 1000°C and a cooling rate of 1.0°C/sec. Apparently, the time at elevated temperatures was not sufficient to cause complete recovery of the strain.

It is believed that the kinetics of recovery for the 20% prior strain samples was greater than that for the 10% prior strain samples (as indicated by the EPR-DOS and TG precipitation evidence presented earlier). This would explain why the sensitization enhancement of the MA material with 20% prior strain was not much greater than that for 10% prior strain at slow cooling rates and peak temperatures of 950°C and below. In fact, the 20% prior strain samples provided less

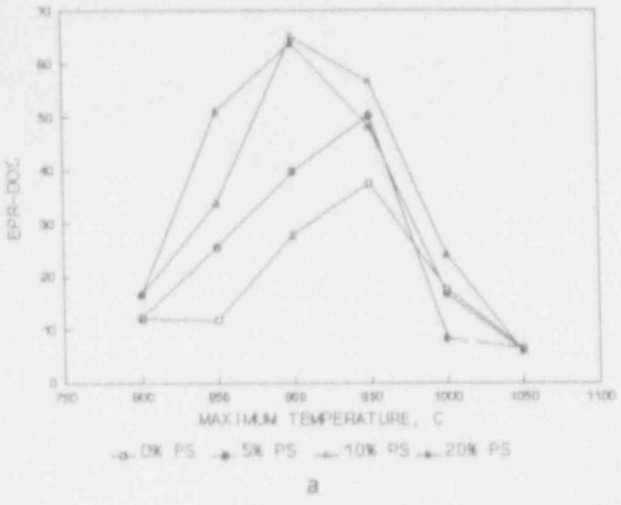

a

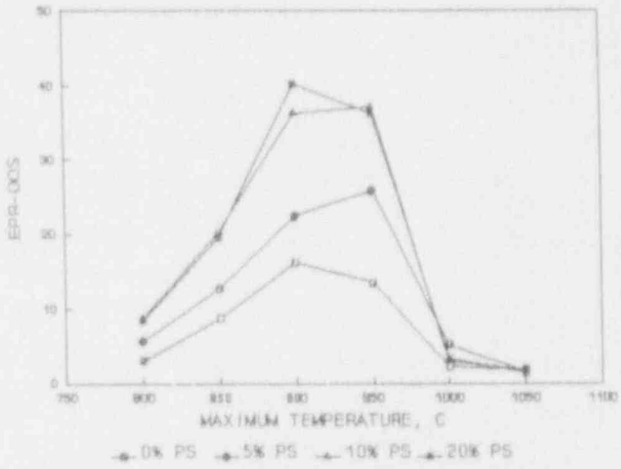

b

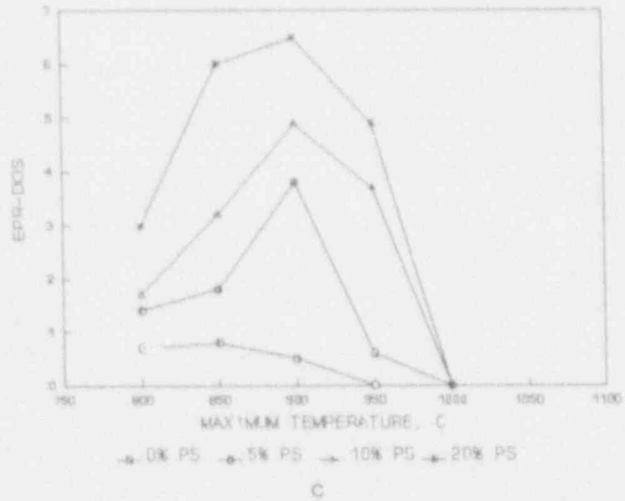

c

Figure 10. Measured EPR-DOS Values for Mill Annealed Material and Prestrained Alloy 17 Material as a Function of Peak Temperature and Cooling Rate: a) Cooling rate = 0.05 C/sec; b) Cooling rate = 0.1°C/sec; c) Cooling rate = 1°C/sec.

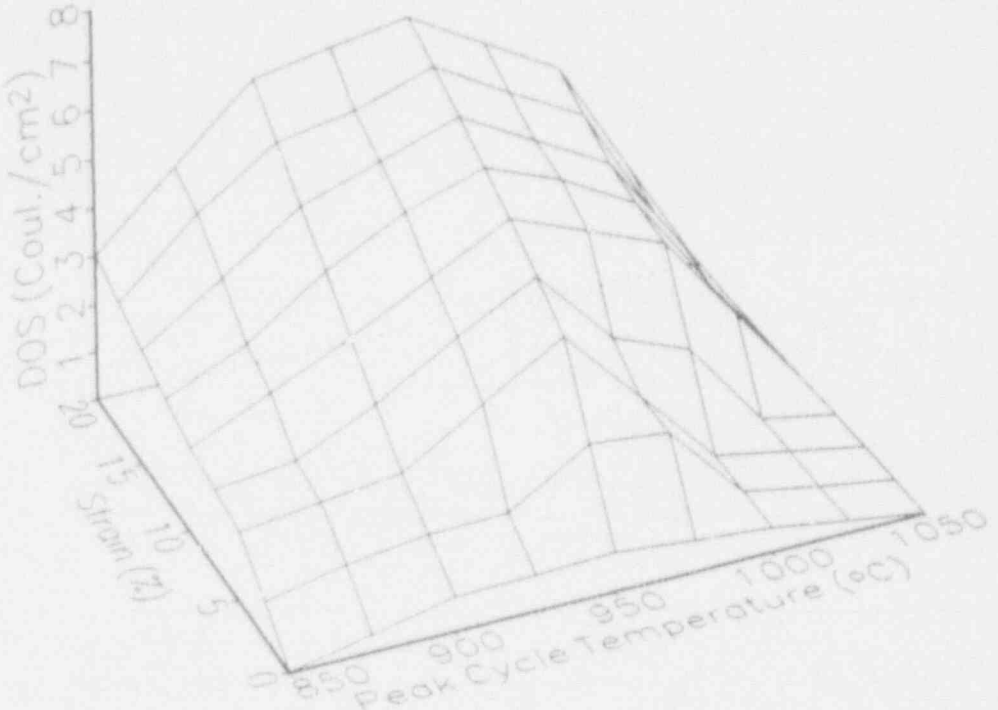

Figure 11. Three-Dimensional Surface Map of Prior Strain Effects on CC sensitization Behavior for Alloy 17 at a Cooling Rate of 1.0°C/s.

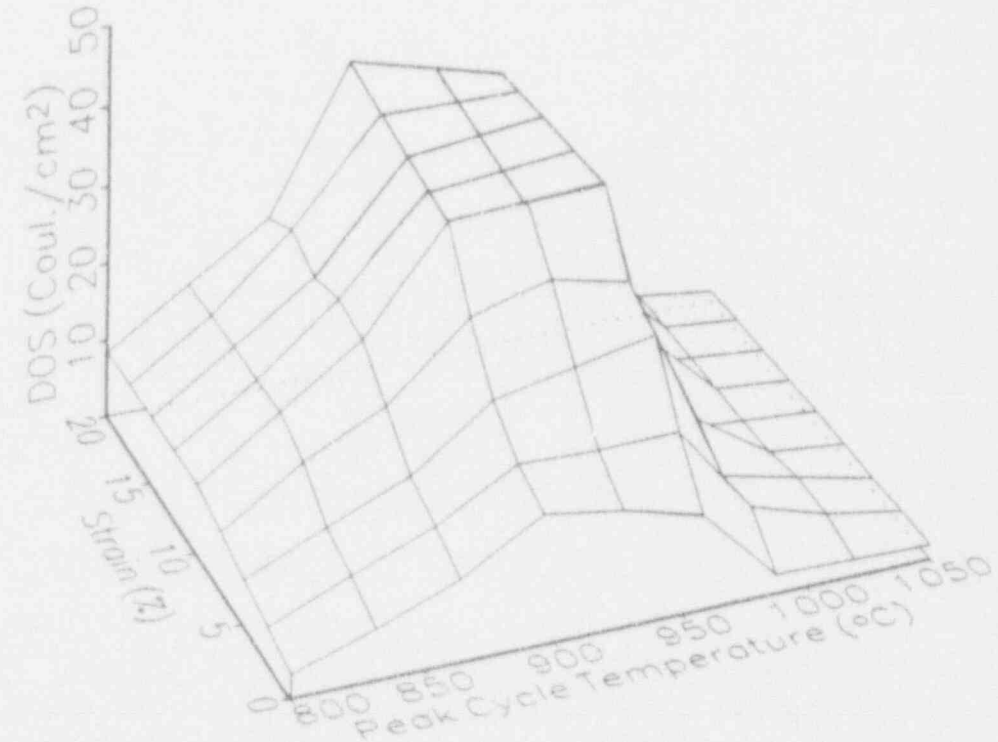

Figure 12. Three-Dimensional Surface Map of Prior Strain Effects on CC sensitization Behavior for Alloy 17 at a Cooling Rate of 0.1°C/s.

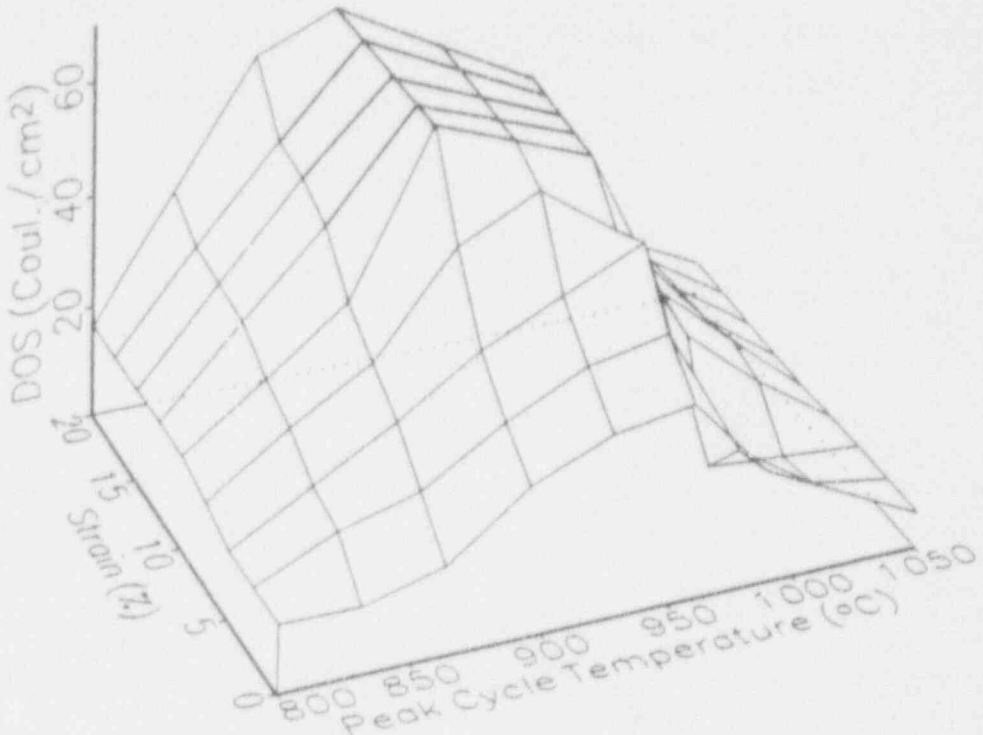

Figure 13. Three-Dimensional Surface Map of Prior Strain Effects on CC sensitization Behavior for Alloy 17 at a Cooling Rate of 0.5°C/s.

enhancement of sensitization than did the 10% prior strain samples for a cooling rate of 0.05°C/sec at peak temperatures of 900°C and 950°C. This is believed to be due to the recovery process. Apparently, there is a complicated correlation between the amount of prior deformation, peak cycle temperature, time spent at elevated temperatures, and the amount of recovery that takes place in the strained specimens. All of these factors influence the effect of prior deformation on the enhancement of sensitization.

As mentioned previously, the 20% strain samples subjected to peak temperatures of 800°C, 850°C, and 900°C (for cooling rates of 0.10°C/sec and 0.05°C/sec) did exhibit some TG attack after EPR testing. However, these were the only specimens that showed TG attack after EPR testing. Therefore, the EPR-DOS results shown for these samples slightly overestimate the actual grain boundary chromium-depletion.

Quantification of sensitization using EPR-DOS values can be rendered invalid if large amounts of transgranular precipitation are present. This is because the method used to normalize the integrated charge value (Q) by the grain boundary area of the sample to obtain the EPR-DOS as outlined previously relies upon all of the attack during the EPR test being uniform and specific to the grain boundaries. Therefore, if a large amount of TG carbide is present and results in TG attack during testing, the EPR-DOS value obtained is no longer representative of Cr-depletion conditions at the grain boundaries. This is not considered to be a factor in the present work since the TG attack observed was minor and only occurred for a few thermal treatments.

3.4 Prestrain Effect on Alloy 17 Sensitization Development During the Cooling Cycle

Sensitization development of MA and prestrained MA (10% prior strain) samples, heated to a peak temperature of 950°C and slow cooled at a rate of 0.05°C/sec, are compared in Figure 14. Deformation was found to significantly enhance the sensitization development of the MA material throughout the CC sensitization temperature regime (at least down to 600°C). A small, but equal amount, of sensitization was found to have developed in MA and 10% prior strain samples cooled to a minimum temperature of 900°C. This result is not surprising since the EPR-DOS values obtained for a sample quenched from a high peak temperature such as 900°C are primarily controlled by the minimum grain boundary Cr concentration which is expected to be high and limit DOS values. However, the results do indicate that carbide precipitation and more importantly, sensitization, occurred at relatively high temperatures, that is between 950 and 900°C, for both MA and prestrained materials.

Prestrained MA samples had EPR-DOS values higher than MA samples for all minimum temperatures of 850°C and below. As cooling progressed to lower temperatures, the difference in EPR-DOS values between the prestrained and MA samples became larger. This is evidence that strain had a significant effect on the kinetics of carbide growth and sensitization development for temperatures at least as high as 850°C.

3.5 Discussion of Effects of Prior Deformation on Continuous Cooling Sensitization

In the current work, enhancement of sensitization development due to prior strain has been quantitatively mapped as a function of cooling rate and peak cycle temperature for prior strains up to 20%. Strain recovery has been shown to be a factor in reducing the effect of strain on sensitization enhancement, especially for peak temperatures above the critical peak temperature. Results reported previously on the effects of strain on CC sensitization have, in some cases, been contradictory and were not as quantitative as the current results.[17,18,22]

In a previous study, Solomon[17] reported that 5% prior strain was required to enhance CC sensitization but that strains of up to 25% did not have any greater enhancing effects than 5%. This is in contrast to the current study in which DOS development increased with increasing prior deformation. Solomon also reported that sensitization development in another heat of 304 SS was not enhanced by 10% strain. These results may suggest that heat-to-heat variations in SSs exist and can affect the observed CC sensitization response of annealed and strained materials. However, in the case of 5% versus 25% prior strain, the technique Solomon used for measuring DOS may have had an effect on the results obtained. One factor which may have hindered the quantification of sensitization for Solomon's research was that the modified Strauss test was used for DOS determination. Although the modified Strauss test has been found to correlate well with grain boundary Cr-depletion, it is not fully quantitative, not a suitable method for detecting very low degrees of sensitization, and may be ineffective for samples with very high DOS values in which penetration of the sample reached 100%.[9,23]

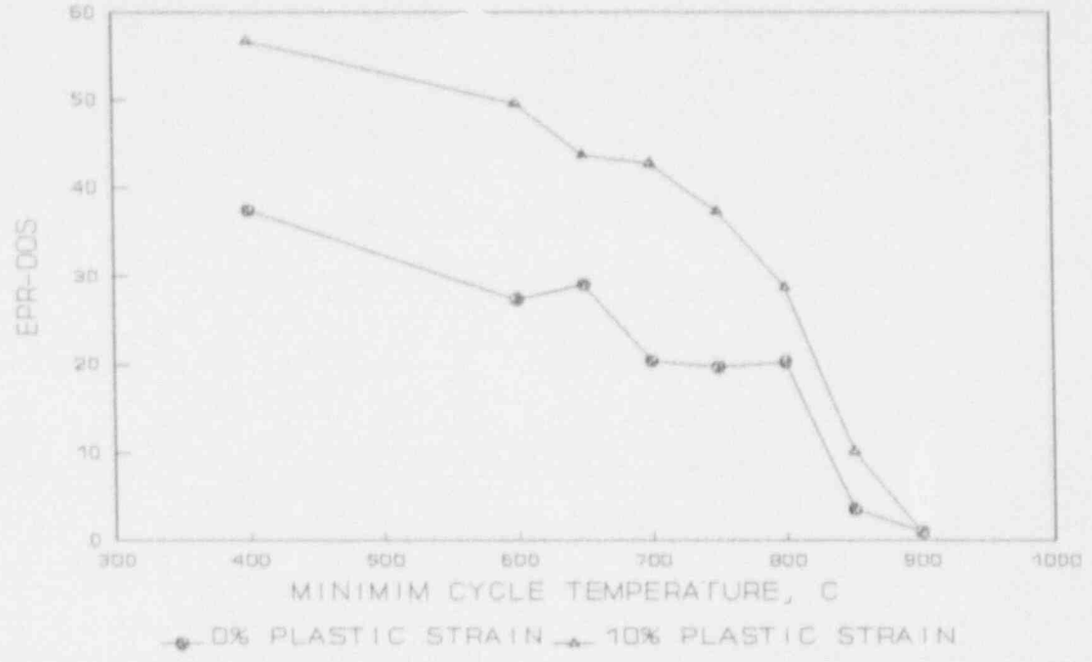

Figure 14. Measured Sensitization Development for Mill Annealed Alloy 17 Material During Linear Cooling from a Peak Temperature of 950°C at a Cooling Rate of 0.05°C/sec.

4.0 SENSITIZATION MODELING

Sensitization modeling is based on diffusional concepts which allow prediction of grain boundary chromium depletion, as defined by a chromium minimum and chromium depletion profile as a function of distance away from the grain boundary. It is possible to experimentally measure the exact chromium depletion profile using the scanning transmission electron microscope (STEM) and this has been done for many specimens as a function of heat treatment and composition.[2-4,25-27] However, STEM analysis techniques are not applicable to large test matrix analysis. Thus the majority of sensitization measurements were carried out using the EPR test. This test was specifically developed to detect and quantify the presence of chromium depletion regions, as mentioned above. An empirical correlation between measured STEM chromium depletion and EPR-DOS allowed model predictions of EPR-DOS from basic predictions of chromium depletion.[2,3,26,27]

4.1 Continuous Cooling Model Development

The SSDOS model treated continuous cooling induced sensitization development as step-wise isothermal sensitization development.[4] Small isothermal steps (determined based on cooling rate) at average temperatures were used to calculate total sensitization development. Cumulative sensitization from previous steps was first determined. Then sensitization at the active step was determined from the known initial sensitization level and the time at the active isothermal step. This new sensitization value was then input as the initial sensitization level for the next isothermal step.

The time at the active isothermal temperature needed to achieve the initial cumulative sensitization value was back calculated and then added to the hold time at the active isothermal temperature to yield an "effective" hold time. A new cumulative sensitization value is then calculated from this effective total hold time at the given active isothermal temperature. The accelerating effect of plastic strain was taken into account by simply multiplying chromium diffusivity by an empirically derived factor proportional to total strain.[2-4]

Predictions of continuous cooling sensitization development were made using SSDOS and compared with actual continuous cooling data developed using a Gleeble, equipment specifically developed for thermomechanical cycle simulation, as previously discussed. Comparison between predicted and measured EPR-DOS indicated that SSDOS consistently over predicted sensitization development, Figure 15a.[6] The probable cause is the assumption of instantaneous carbide precipitation and development of minimum chromium grain boundary levels.

A more accurate prediction of continuous cooling sensitization was obtained by insertion of a module to predict nucleation time. This module was developed based on the assumption that carbides must first nucleate at sufficient density on the grain boundary prior to that boundary reaching an "equilibrium" chromium minimum. Chromium depletion calculations are not initiated until this nucleation time is reached.

A nucleation module for isothermal DOS development for SSDOS was first developed by Bruemmer based on homogeneous nucleation theory.[2] The module was subsequently modified by Advani to conform to heterogeneous nucleation theory.[8] This latter nucleation modeling approach was used by Li to develop the SSDOS-I continuous cooling nucleation module.

It is still assumed that the chromium minimum concentration is instantaneously arrived at over the complete boundary once initial nucleation takes place. A more realistic assumption would be that this minimum concentration is, at least initially, only effective a given distance from the carbide site, and that this effective distance is a function of time and temperature. In addition, boundary-to-boundary variation would also have to be accounted for.

Calculation of nucleation time is carried out in essentially the same step-wise manner as sensitization development using the Manning-Loring method.[2,3] A nucleation fraction, based on total isothermal nucleation time at the active isothermal step, is calculated for each isothermal time step; step fractions are summed until a nucleation fraction of one is reached. Nucleation is then assumed to be complete and chromium depletion calculations are initiated.

Improved predictions of continuous cooling sensitization was obtained with the modified model SSDOS-I. Comparisons with experimental data and SSDOS predictions, Figures 16 through 19, indicate that SSDOS-I comes closer to predicting experimental data than SSDOS. Comparison of both model version predictions to actual measured values is presented in Figure 15. The SSDOS-I either tends to straddle the 45° line or predict too low DOS values while SSDOS is consistently above the 45° line.

Improved predictions of continuous cooling sensitization was obtained with the modified model SSDOS-I, however, an unacceptable number of predictions generated DOS values that were too low, see Figure 15b. This lead to the further modification of the SSDOS-I nucleation module based on a best-fit-to-data basis and resulted in development of SSDOS-II. Comparisons with experimental data, Figures 20 through 23, indicate that SSDOS-II comes much closer to predicting experimental data than SSDOS-I. Overall comparison of all three model version predictions to actual measured values is presented in Figure 15. The SSDOS-II tends to straddle the 45° line while SSDOS is consistently above the 45° line and the SSDOS-I tends to under predict.

The discussion to date, although it has not been so stated, is only applicable to continuously cooling thermal cycles exhibiting very rapid heating times, relatively short cooling times, and low to intermediate maximum temperatures. The restriction to high heating rate comes from the exclusion of the possibility of nucleation beginning during the heating portion of the thermal cycle. The restriction to relatively short cooling times comes from the fact that excessive carbide precipitation depletes the matrix in carbon and, therefore, increases the equilibrium carbide/matrix minimum chromium concentration and results in desensitization, or "healing". Note that matrix carbide depletion is not expected to occur in welding due to the relatively rapid thermal cycle seen in practical weldment HAZs.

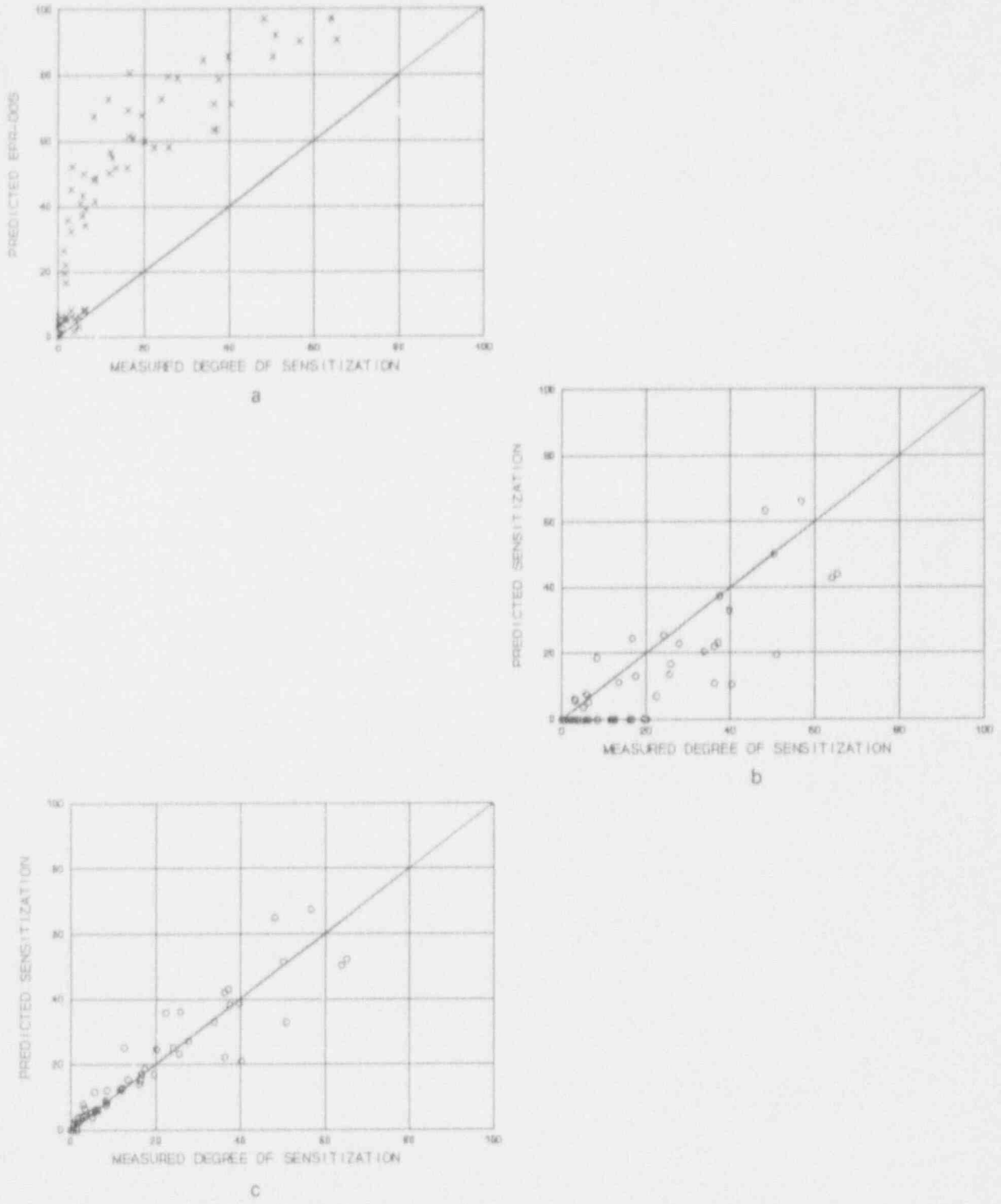

Figure 15. Comparisons Between Measured and Predicted EPR-DOS for Continuous Cooling Results from Mill Annealed and Prestrained Alloy 17 Specimens: a) SSDOS; b) SDOS-I; c) SSDOS-II.

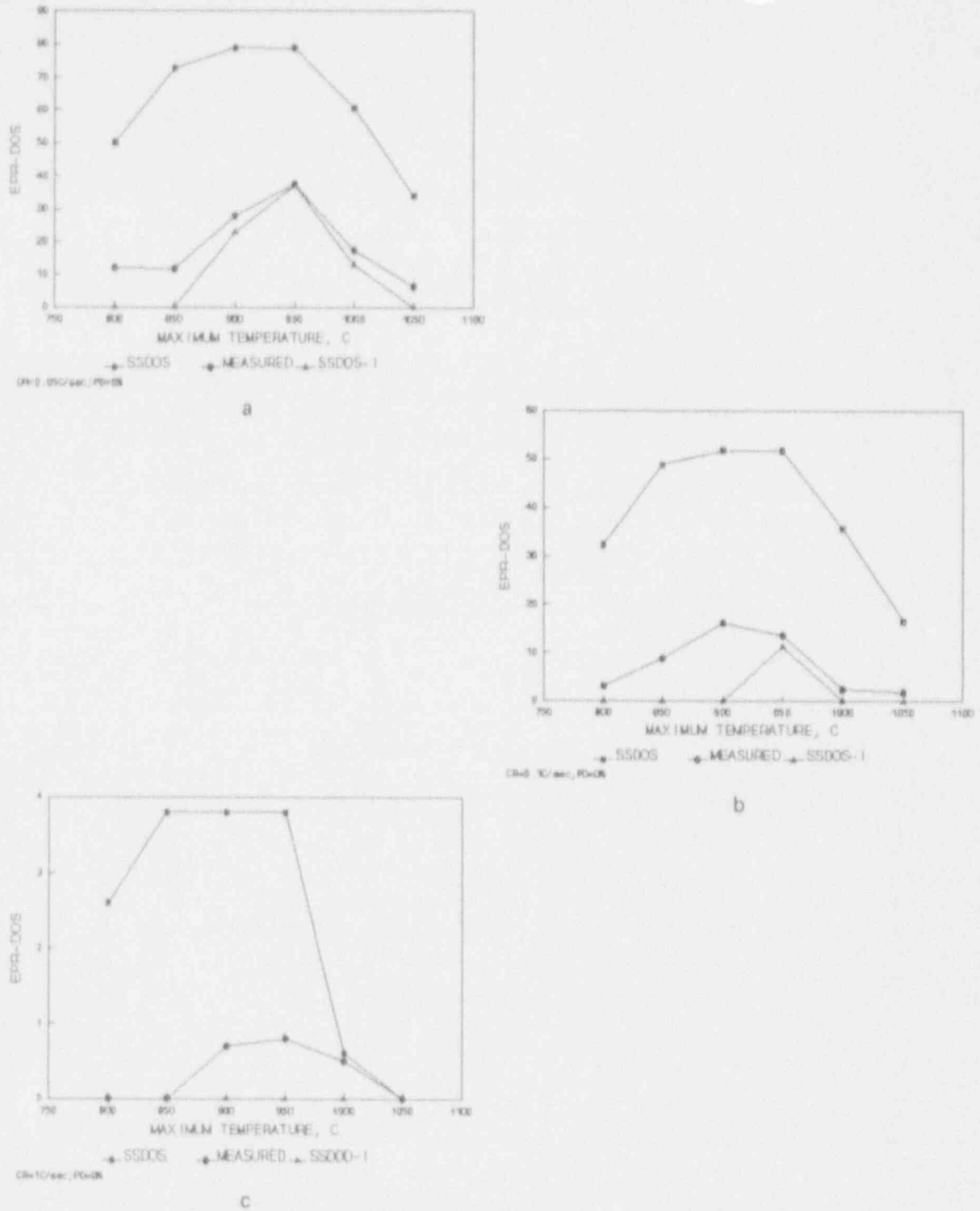

Figure 16. Comparison Between Measured and SSDOS and SSDOS-I Predicted EPR-DOS Values for Mill Annealed Alloy 17 Material as a Function of Peak Temperature and Cooling Rate: a) Cooling rate = 0.05°C/sec; b) Cooling rate = 0.1°C/sec; c) Cooling rate = 1°C/sec.

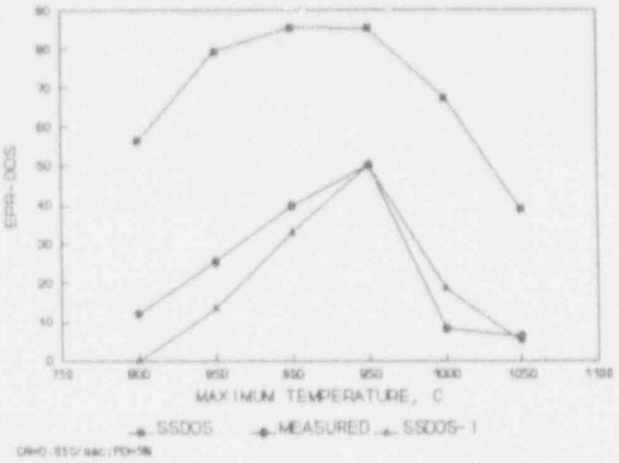

a

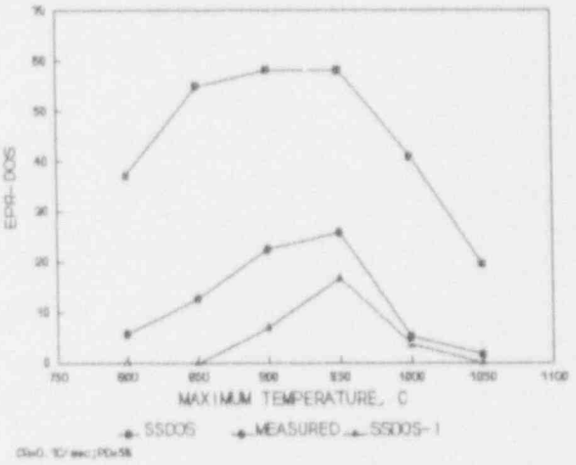

b

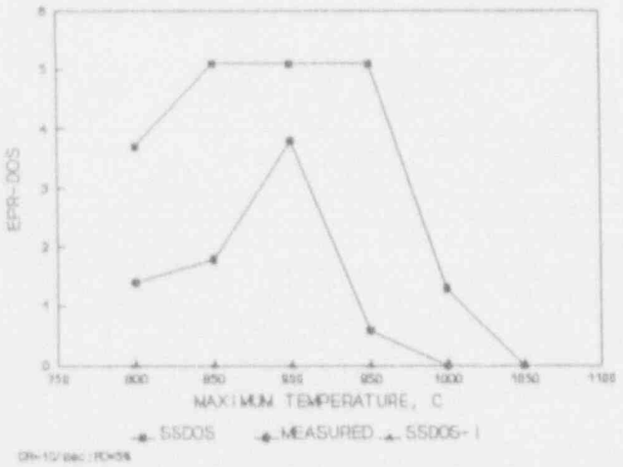

c

Figure 17. Comparison Between Measured and SSDOS and SSDOS-I Predicted EPR-DOS Values for Mill Annealed Alloy 17 Material Prestrained 5% as a Function of Peak Temperature and Cooling Rate: a) Cooling rate = 0.05°C/sec; b) Cooling rate = 0.1°C/sec; c) Cooling rate = 1°C/sec.

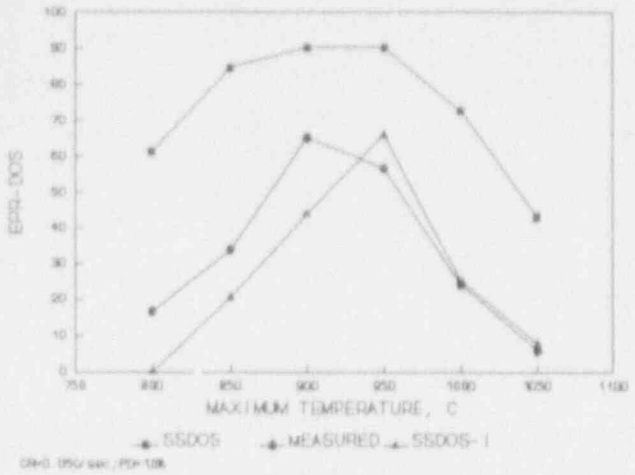

a

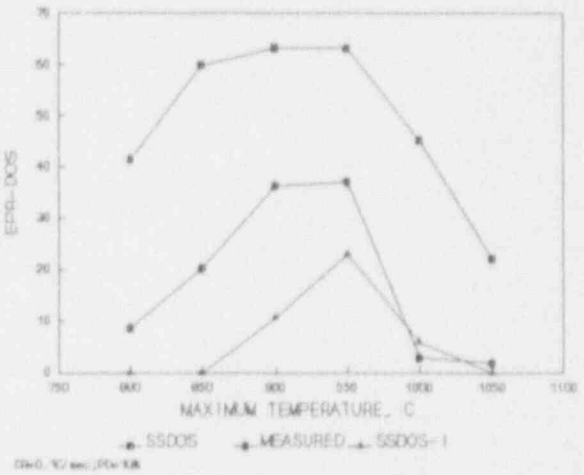

b

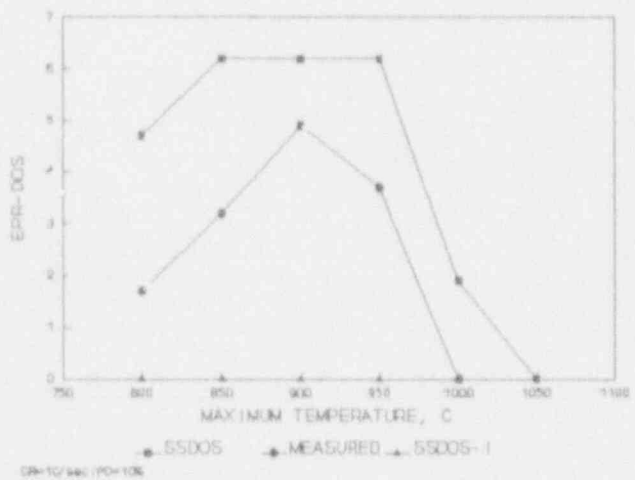

c

Figure 18. Comparison Between Measured and SSDOS and SSDOS-I Predicted EPR-DOS Values for Mill Annealed Alloy 17 Material Prestrained 10% as a Function of Peak Temperature and Cooling Rate: a) Z Cooling rate = 0.05°C/sec; b) Cooling rate = 0.1°C/sec; c) Cooling rate = 1°C/sec.

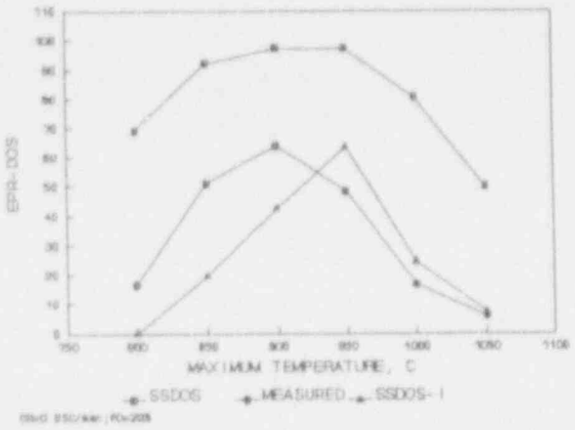

a

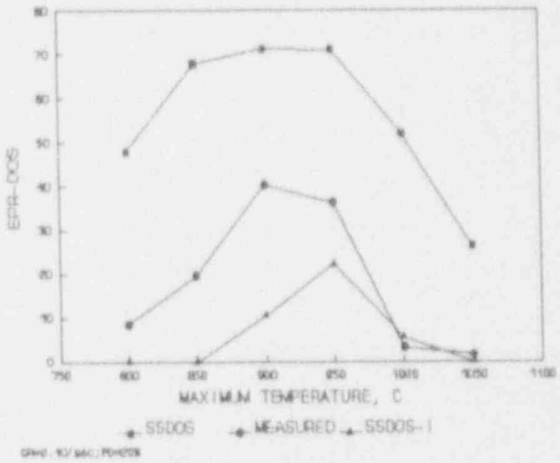

b

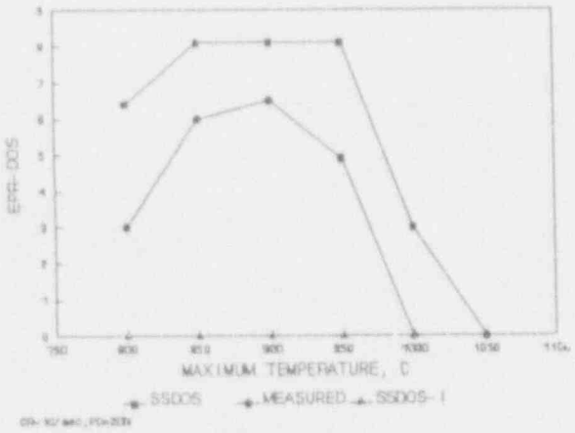

c

Figure 19. Comparison Between Measured and SSDOS and SSDOS-I Predicted EPR-DOS Values for Mill Annealed Alloy 17 Material Prestrained 20% as a Function of Peak Temperature and Cooling Rate: a) Cooling rate = 0.05°C/sec; b) Cooling rate = 0.1°C/sec; c) Cooling rate = 1°C/sec.

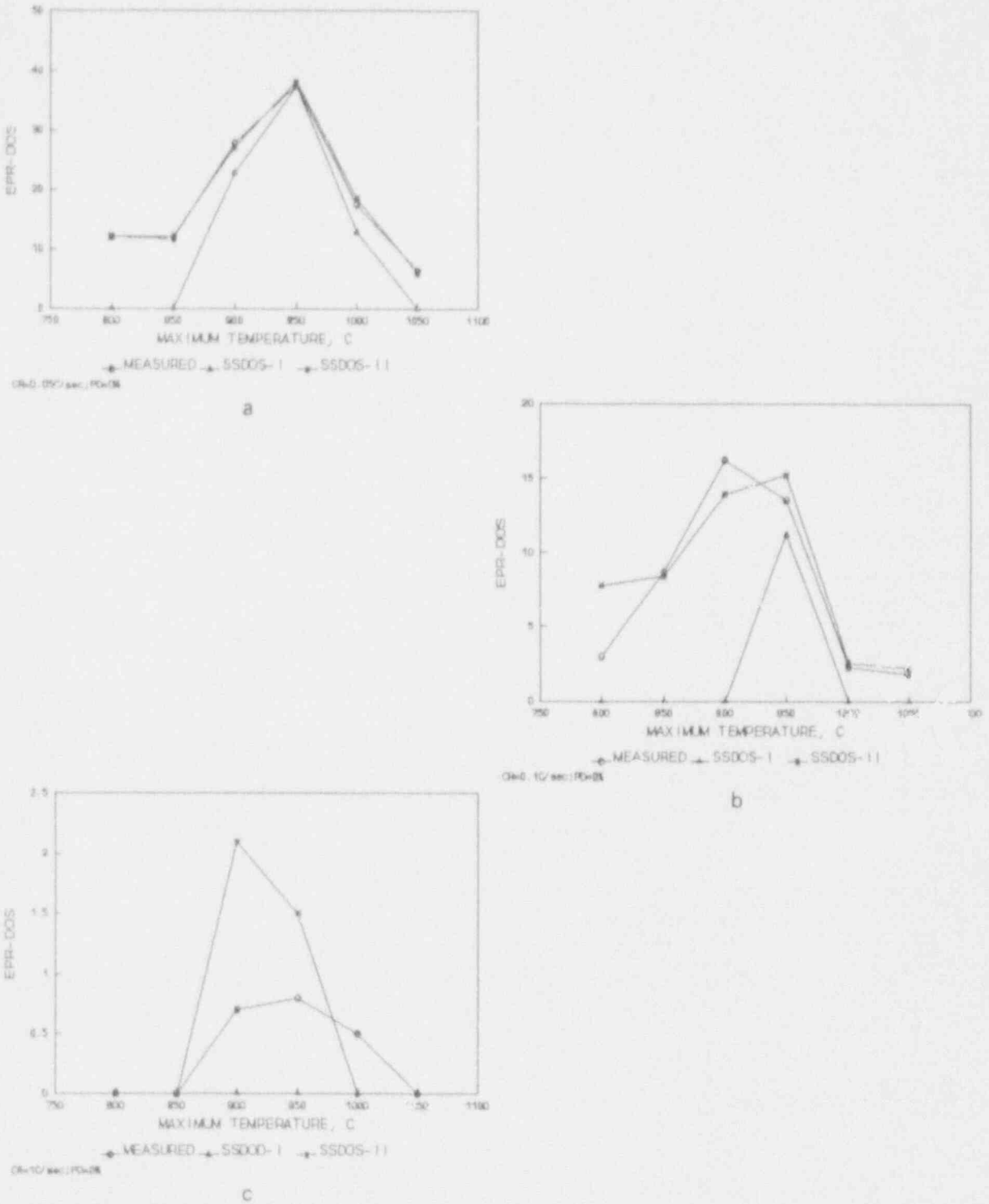

Figure 20. Comparison Between Measured and SSDOS and SSDOS-II Predicted EPR-DOS Values for Mill Annealed Alloy 17 Material as a Function of Peak Temperature and Cooling Rate: a) Cooling rate = 0.05°C/sec; b) Cooling rate = 0.1°C/sec; c) Cooling rate = 1°C/sec.

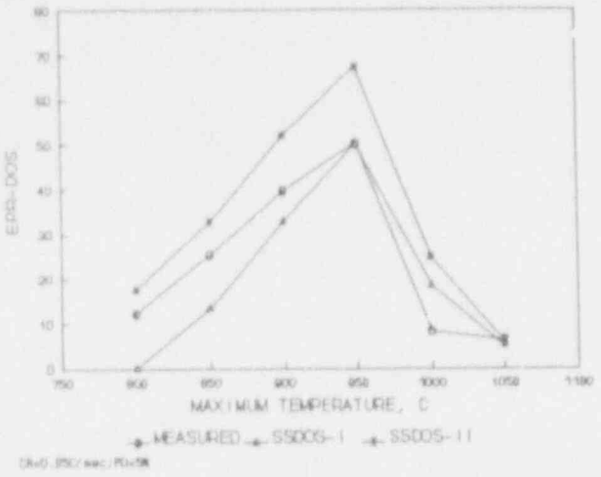

a

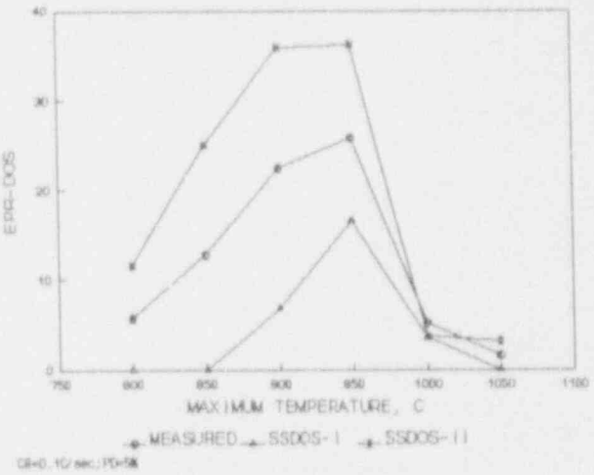

b

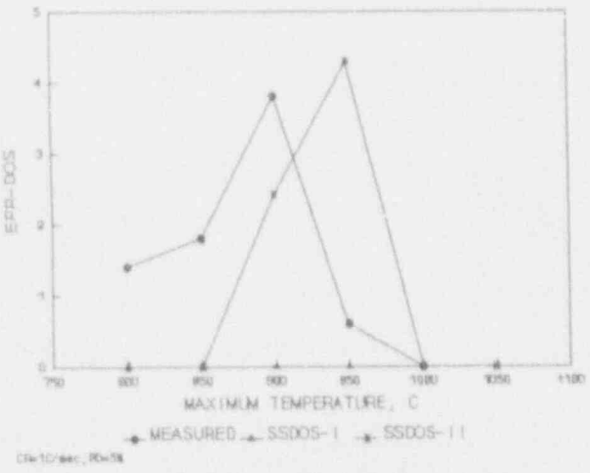

c

Figure 21. Comparison Between Measured and SSDOS-I and SSDOS-II Predicted EPR-DOS Values for Mill Annealed Alloy 17 Material Prestrained 5% as a Function of Peak Temperature and Cooling Rate: a) Cooling rate = 0.05°C/sec; b) Cooling rate = 0.1°C/sec; c) Cooling rate = 1°C/sec.

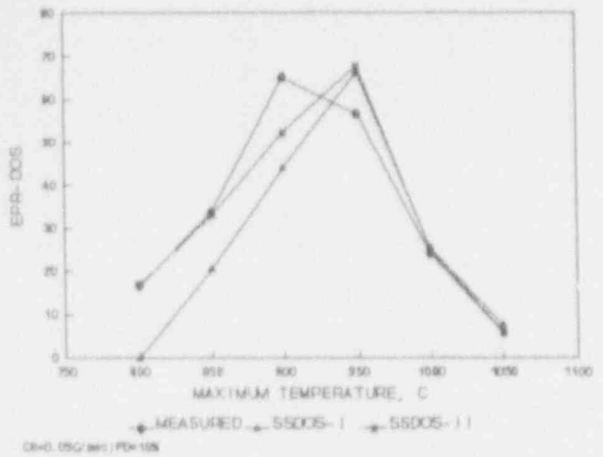

a

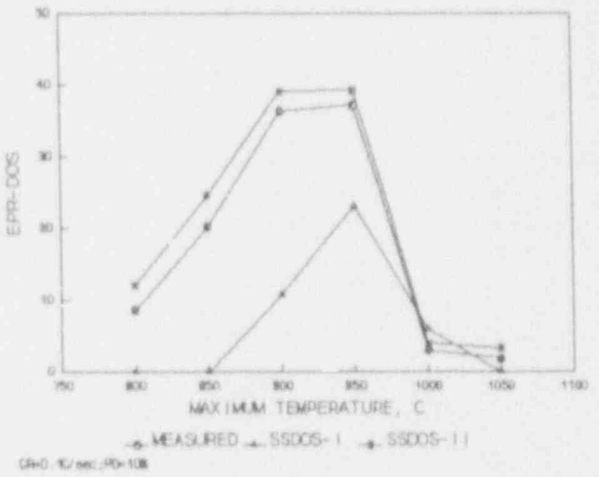

b

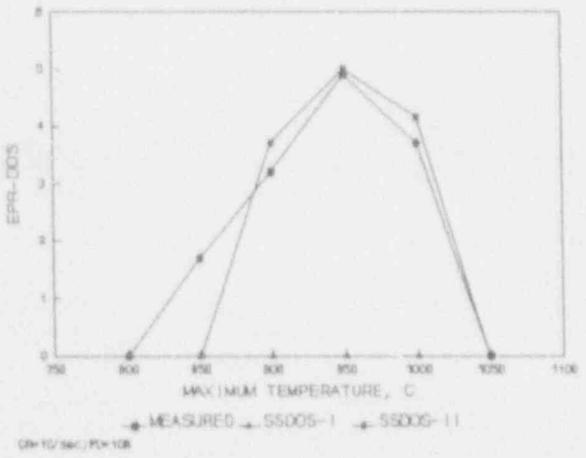

Figure 22. Comparison Between Measured and SSDOS-I and SSDOS-II Predicted EPR-DOS Values for Mill Annealed Alloy 17 Material Prestrained 10% as a Function of Peak Temperature and Cooling Rate: a) Cooling rate = 0.05°C/sec; b) Cooling rate = 0.1°C/sec; c) Cooling rate = 1°C/sec.

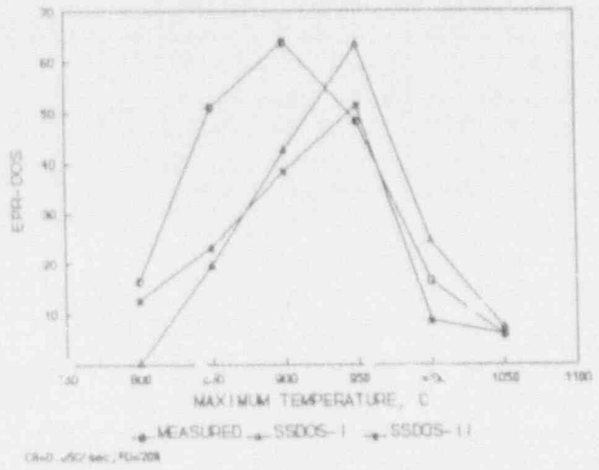

a

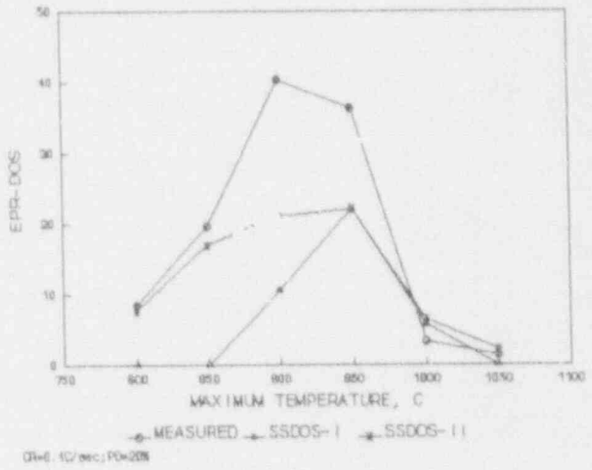

b

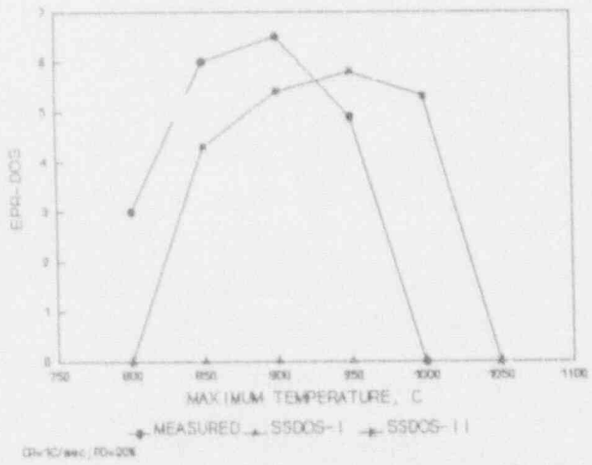

c

Figure 23. Comparison Between Measured and SSDOS-I and SSDOS-II Predicted EPR-DOS Values for Mill Annealed Alloy 17 Material Prestrained 20% as a Function of Peak Temperature and Cooling Rate: a) Cooling rate = 0.05°C/sec; b) Cooling rate = 0.1°C/sec; c) Cooling rate = 1°C/sec.

The restriction to low and intermediate temperatures comes from the experimentally observed fact that sensitization development induced at a constant cooling rate increases up to a given critical temperature (range) and then precipitously drops, Figure 24.[5] It should be emphasized that this drop takes place even though the material heated above this critical temperature undergoes exactly the same cooling time/temperature thermal cycle once it reaches the critical temperature as the material only heated up to the critical temperature. Previous work, Figure 9, indicates that a distinct change in kinetics occurs upon heating SS above a given critical temperature.[21]

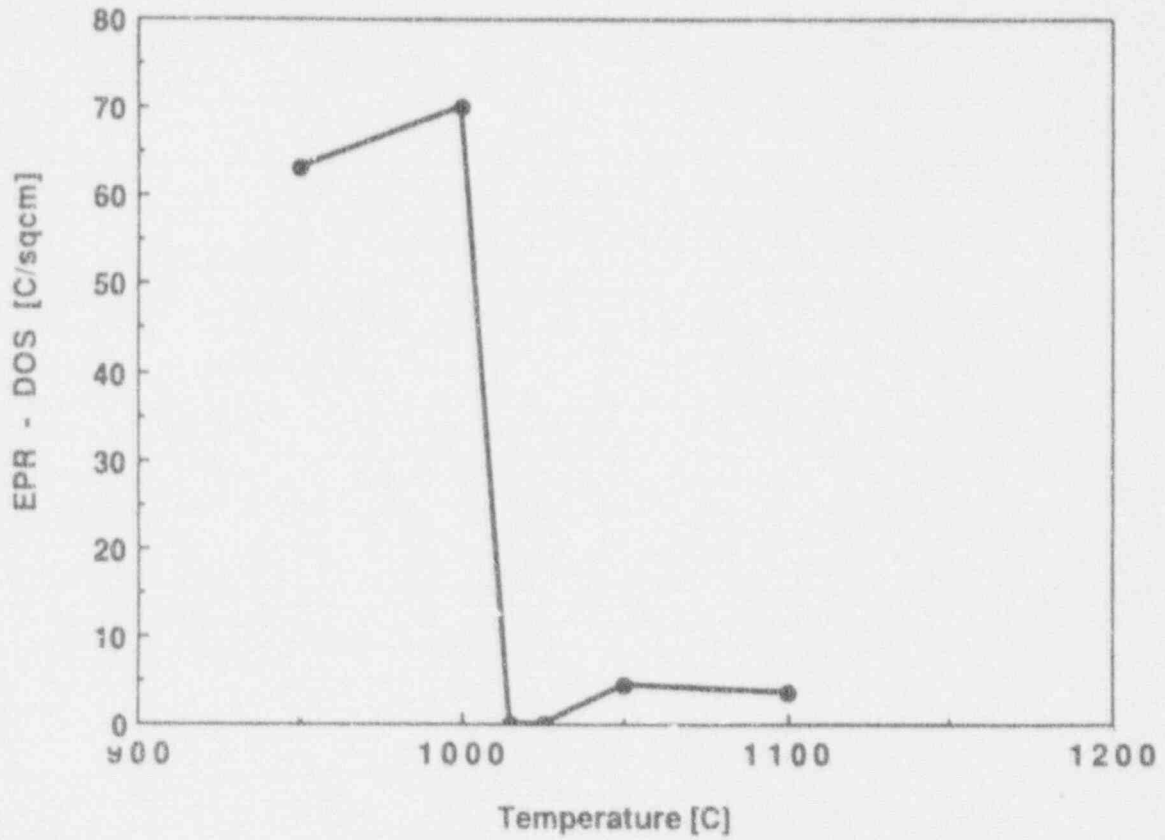

Figure 24. Change in Sensitization Induced by Continuous Cooling as a Function of Maximum Temperature.

This problem was addressed in SSDOS by assuming a change in kinetics once the material went above a critical temperature (approximately 1000°C, depending on material carbon composition); kinetics were changed by a decrease in effective chromium diffusivity.[2,4] This change in diffusivity was empirically determined based on limited continuous cooling data. Both the change in kinetics and estimation of the appropriate temperature to initiate the change in kinetics are approached differently in SSDOS-I and -II. The temperature needed to be reached to initiate kinetics change is assumed to be related to the carbon solid solubility temperature based on reported solubility expressions, as illustrated in Figure 7.[20] This treatment assumes that carbon atoms precipitated at, or segregated to, grain boundaries at temperatures below the solid solubility temperature reduce nucleation times over "clean" grain boundaries heated into the solid solubility region.

The exact effective grain boundary dissolution temperature is probably greater than the equilibrium solubility temperature and will be a function of heating rate. However, as the present experimental data is insufficient to quantitatively assess this phenomenon, the model simply assumes the kinetic change takes place when the material is heated above the solid solubility temperature. These equations are input into the model as a function temperature and alloy composition.

The nucleation kinetics changes in SSDOS-II for material heated below and above the solid solubility temperature are based on changes in nucleation time; the effective diffusivity of chromium is assumed to remain unchanged. The SSDOS-II predictions of nucleation time as influenced by maximum temperature is illustrated in Figure 25. The quantitative kinetic changes used in SSDOS-II were developed using data best fit techniques; the resultant agreement with experimental data can be seen in Figures 20 through 23.

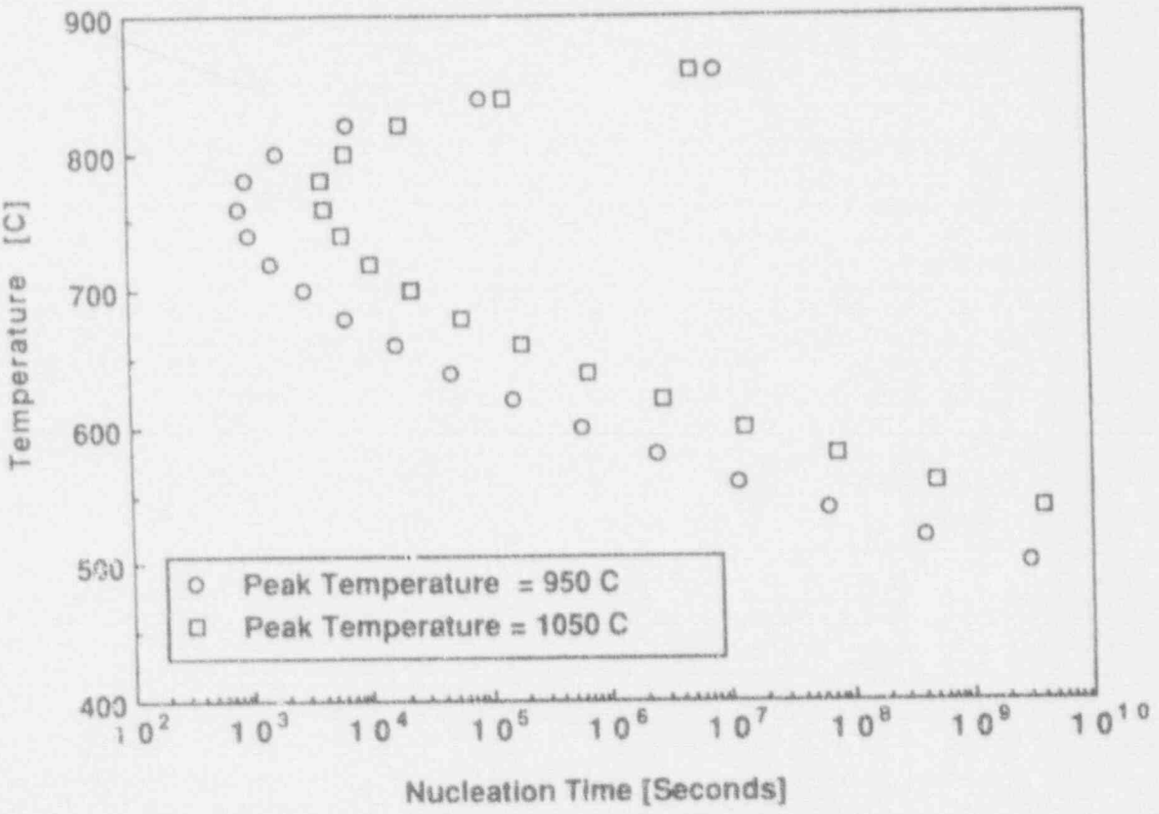

Figure 25. Change in Predicted Nucleation Time as Function of Continuous Cooling Cycle Peak Temperature.

4.2 Comparison of Prediction Reality

It can be seen (Figure 15) that, in general, both SSDOS and SSDOS-II predict increasing DOS values with decreasing cooling rate, which agrees with experimental data. However, SSDOS predicts higher EPR-DOS values and less effect of peak temperature then seen experimentally, Figures 16 through 19. The SSDOS-II model predictions appear to exhibit EPR-DOS values, in general, relatively close to observed values and also exhibit EPR-DOS changes as a function of peak temperature that correspond closely to those seen experimentally, Figures 20 through 23.

The generic SSDOS-II predictions illustrated in Figures 20 through 23 appear to be reasonable and to account in a reasonably correct way for the effect of plastic deformation. However, if one assesses the effect of deformation independently from other effects one finds distinct prediction trends as a function of degree of plastic deformation. A comparison of SSDOS-II predictions versus measured EPR-DOS for MA Alloy 17 material indicates a good correlation with little scatter, Figure 26a. Assessment of the effect of 5% strain, Figure 26b, indicates that SSDOS-II over predicts the effect of strain, with a possible increase in over prediction with increasing sensitization. The 10% strain results, Figure 26c, exhibit a return to a reasonable prediction capability, with a greater scatter band than exhibited by the MA material. The 20% strain results (Figure 26d) indicate an under prediction, with the possibility of an increasing under prediction with increasing sensitization.

Assessment of predictive capabilities of SSDOS and SSDOS-II as a function of peak temperature and percent prestrain at constant cooling rates are presented in Figures 27 through 28. Figure 27 illustrates that, although SSDOS overpredicts DOS, it does exhibit an increasing DOS with increasing prestrain, as exhibited by the experimental data, Figure 10. The SSDOS-II predictions (Figure 28), in general, exhibit an increasing DOS with increasing prestrain through 10% prestrain and then a decrease in DOS as prestrain is increased from 10 to 20%. Close inspection indicates that the SSDOS-II predictions for 5% prestrain are essentially double the experimentally determined DOS and approximately equal in magnitude to the 10% prestrain SSDOS-II predicted values and the 10% prestrain experimentally determined results. The SSDOS-II 20% prestrain values are close to half of what the experimentally measured values are. The peak DOS predicted values fall between 5 and 10% prestrain while the experimentally measured peak DOS values fall between 10 and 20% prestrain.

Assessment of the experimentally determined effects of 10 and 20% prestrain as a function of peak temperature and cooling rate indicates that DOS increases with increasing prestrain at fast cooling rates but exhibits roughly equal DOS values for 10 and 20% prestrain at slower cooling rates. There appears to be two possible explanations for this behavior. One is that a recovery induced decrease in dislocation density during the longer heat treatment cycles decreases the effectiveness of prestrain of DOS acceleration. A possible rationale for this behavior is that deformation induced dislocation arrays formed due to low levels of prior deformation are stable at (relatively) high temperatures while arrays formed due to high levels of prior strain are subject to recover at intermediate/high temperatures. This would lead to the possibility of enhanced Cr diffusion to grain boundaries due to dislocation piping effects during the complete cycle for low levels of prestrain but decreased enhancement of Cr diffusion at longer times and higher temperatures for higher prestrains. The second possible reason for this

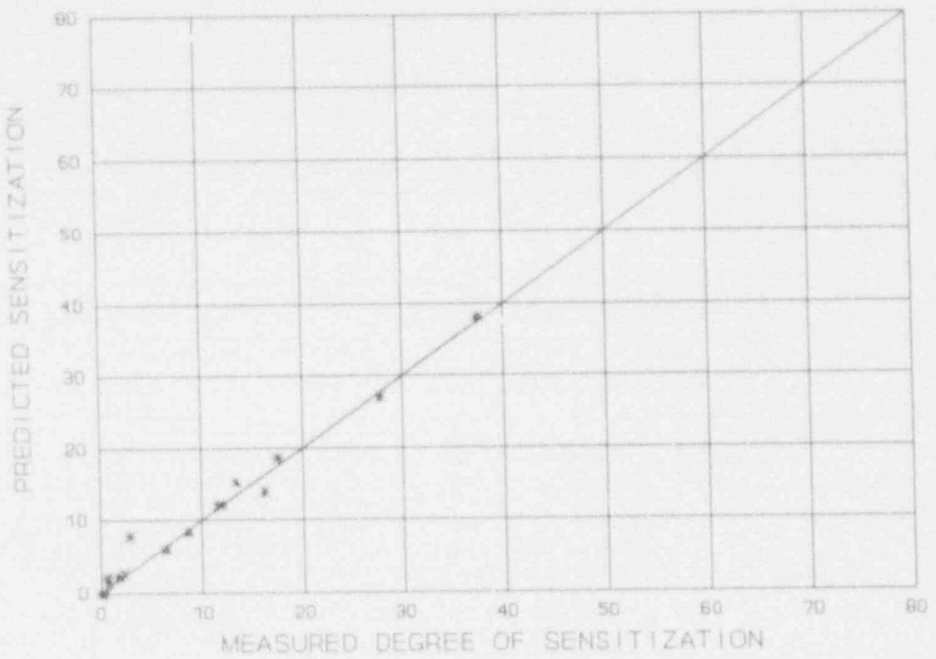

a

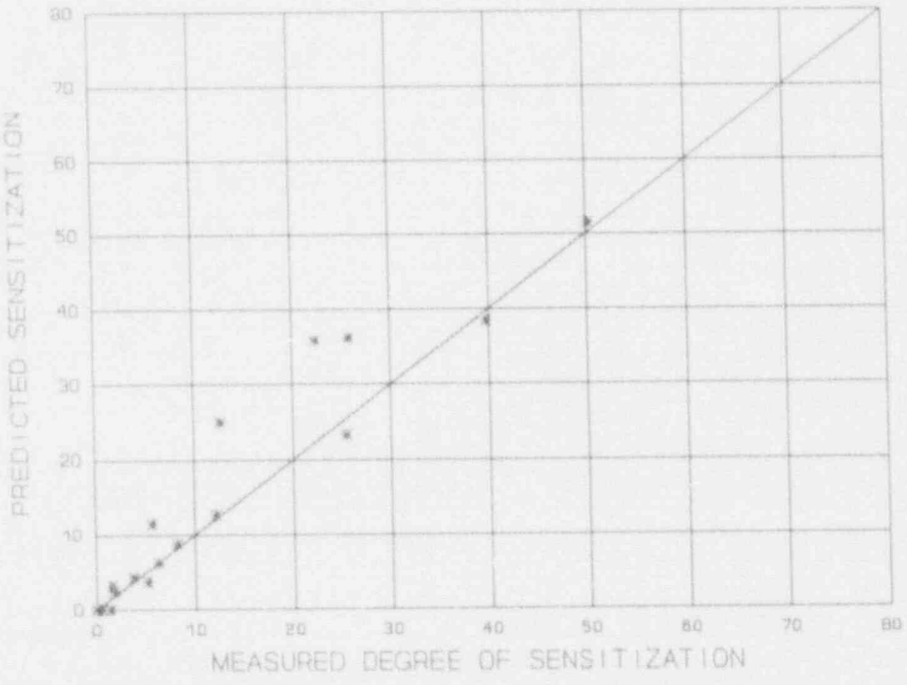

b

Figure 26. Comparison Between Measured and SSDO3-II Predicted EPR-DOS Values for Mill Annealed Alloy 17 Material as a Function of Prestrain: a) 0% Prestrain; b) 5% Prestrain: c) 10% Prestrain; d) 20% Prestrain.

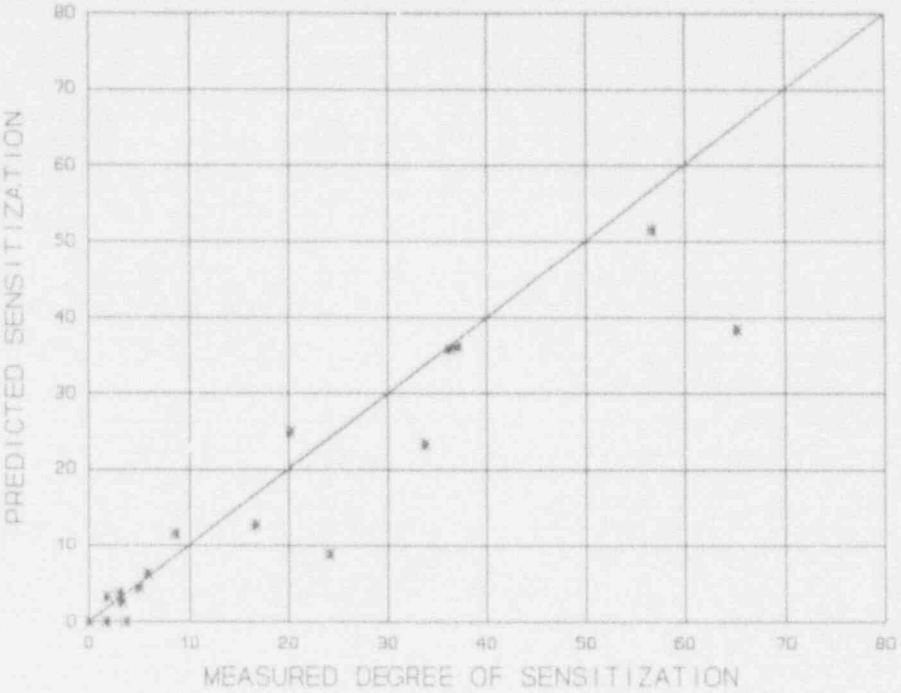

c

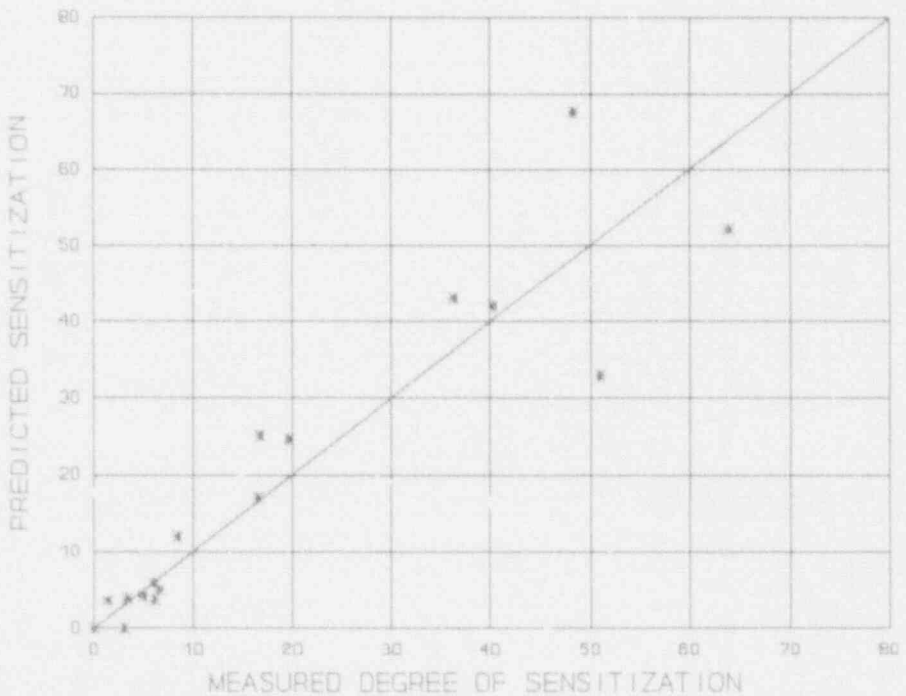

d

Figure 26. Continued.

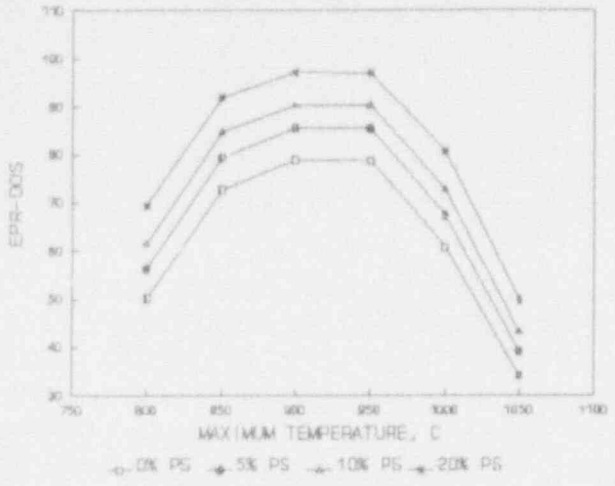

a

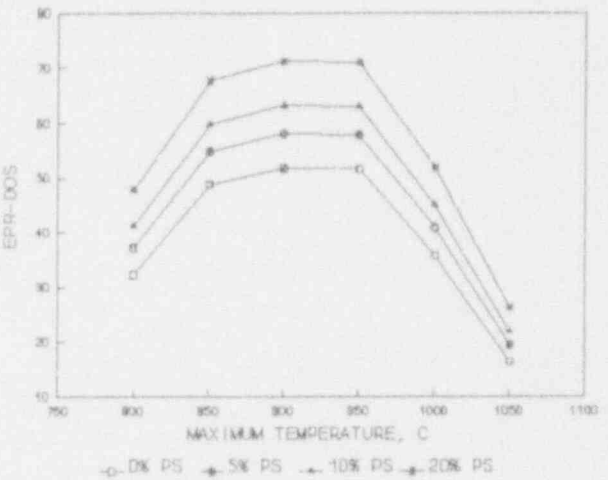

b

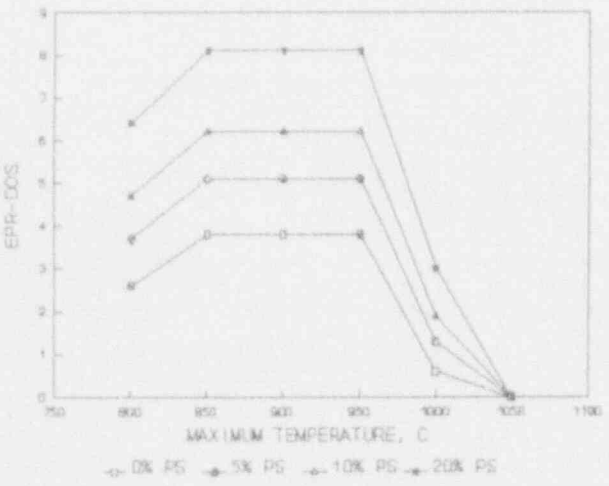

c

Figure 27. SSDOS Predicted EPR-DOS Values for Mill Annealed Alloy 17 Material as a Function of Peak Temperature, Prestrain and Cooling Rate: a) Cooling rate = 0.05°C/sec; b) Cooling rate = 0.1°C/sec; c) Cooling rate = 1°C/sec.

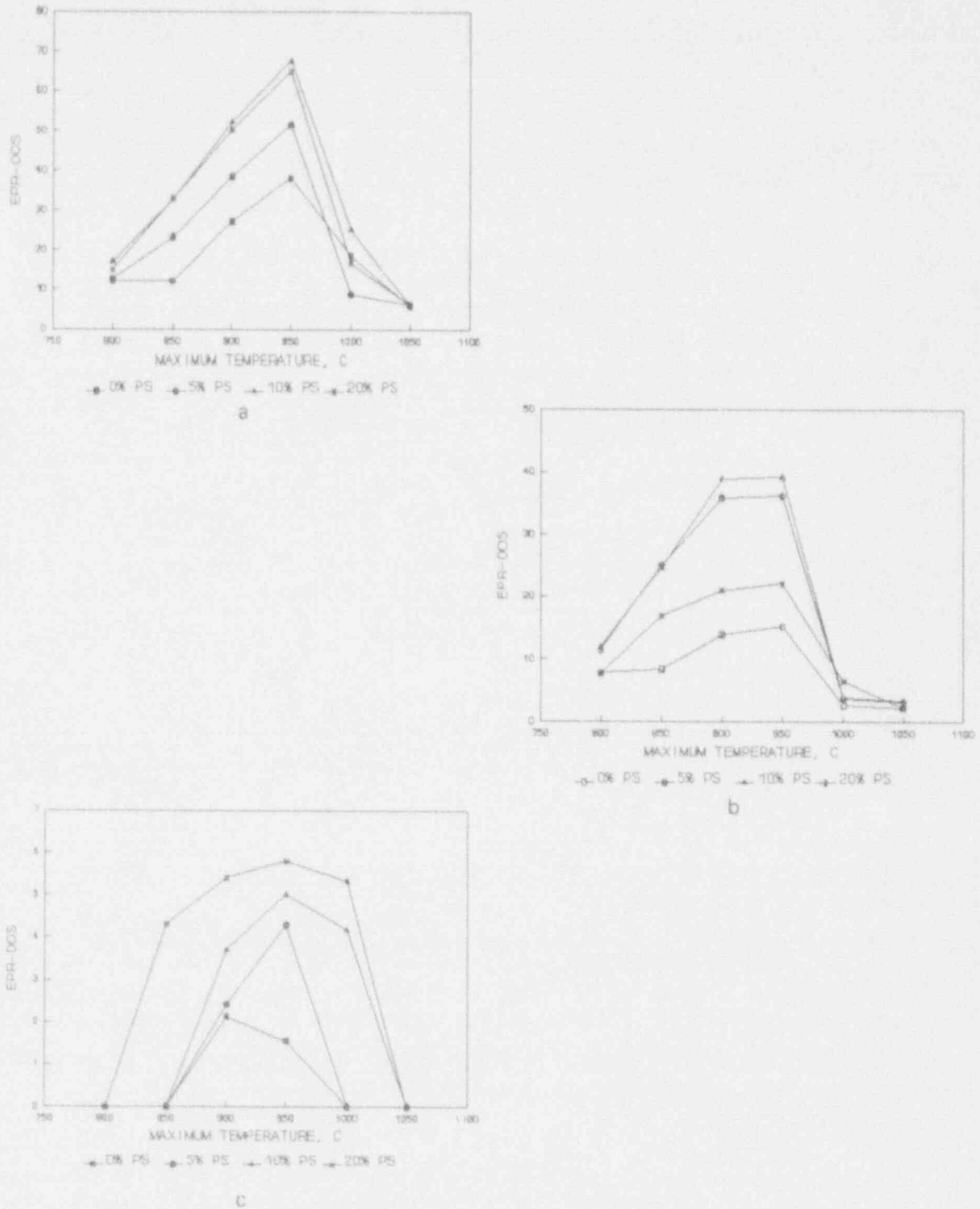

Figure 28. SSDOS-II Predicted EPR-DOS Values for Mill Annealed Alloy 17 Material as a Function of Peak Temperature, Prestrain and Cooling Rate: a) Cooling rate = 0.05°C/sec; b) Cooling rate = 0.1°C/sec; c) Cooling rate = 1°C/sec.

observed phenomenon postulates that no recovery takes place and that accelerated Cr depletion results in matrix carbon depletion resulting in an increase in minimum Cr content at the grain boundaries, thus increasing measured EPR-DOS. Present experimental results are insufficient to determine which mechanism is responsible for the observed decrease in EPR-DOS with increasing prestrain.

It is expected that a relatively simple change in the relationship between prestrain and Cr diffusion acceleration would correct model predictions if the second hypothesis is correct. A more complex relationship would be needed if the first hypothesis is correct. In any case, the data presented above indicates that, for SSDOS-II, the effect of low values of strain are over predicted and high values of strain are under predicted. Thus it appears that the simple linearly increasing effect of strain on DOS development assumed in the SSDOS and SSDOS-II models needs to be modified into a more complex relationship of changing DOS acceleration as a function of prestrain, time and temperature if model predictions are to match experimental results.

The effect of simply assuming the strain induced chromium diffusion function used in SSDOS-II was twice as great as required is illustrated in Figure 29. This figure presents predicted versus measured EPR-DOS for the 10 and 20% prestrain as predicted by "SSDOS-III". The fit appears to be considerably better than that found for SSDOS-II, Figure 27.

4.2.1 Model Application to Sensitization Development During the Cooling Cycle

The previous results indicate that SSDOS-II/SSDOS-III predict final continuous cooling sensitization relatively successfully. The next question is do they predict the development of sensitization for a given thermal cycle as a function of decreasing temperature. A comparison of the prediction capability of SSDOS and SSDOS-II as applied to sensitization development in MA Alloy 17 is presented in Figure 30. The results indicate that SSDOS over predicts EPR-DOS at all cooling cycle temperatures. It does, however, initiate EPR-DOS development at comparable temperature to measured values. The SSDOS-II predictions yield comparable EPR-DOS values to measured values at lower cycle temperature but initiate EPR-DOS development at cooling temperatures below experimentally observed results for all peak temperatures.

The early EPR-DOS development in SSDOS is due to the assumption that carbide growth initiates instantaneously upon reaching the given peak temperature or calculated minimum carbon solid solubility temperature. The delay in SSDOS-II sensitization development is due to the added nucleation module. It appears that the SSDOS-II nucleation module is too conservative and that the subsequent initial sensitization development at intermediate temperatures is too accelerated.

The application of model predictions to Alloy 17 prestrained 10% and then cooled from 950°C at 0.05°C/sec is presented in Figure 31. The results are similar to that found in Figure 30 except that the SSDOS-III predictions yield closer final EPR-DOS values to experimentation than SSDOS-II.

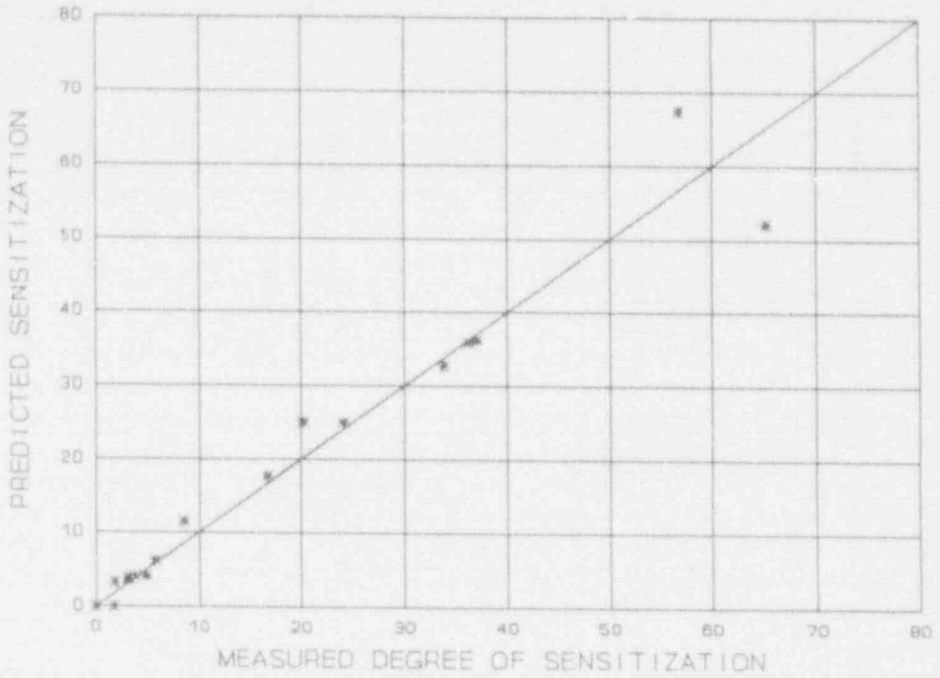

a

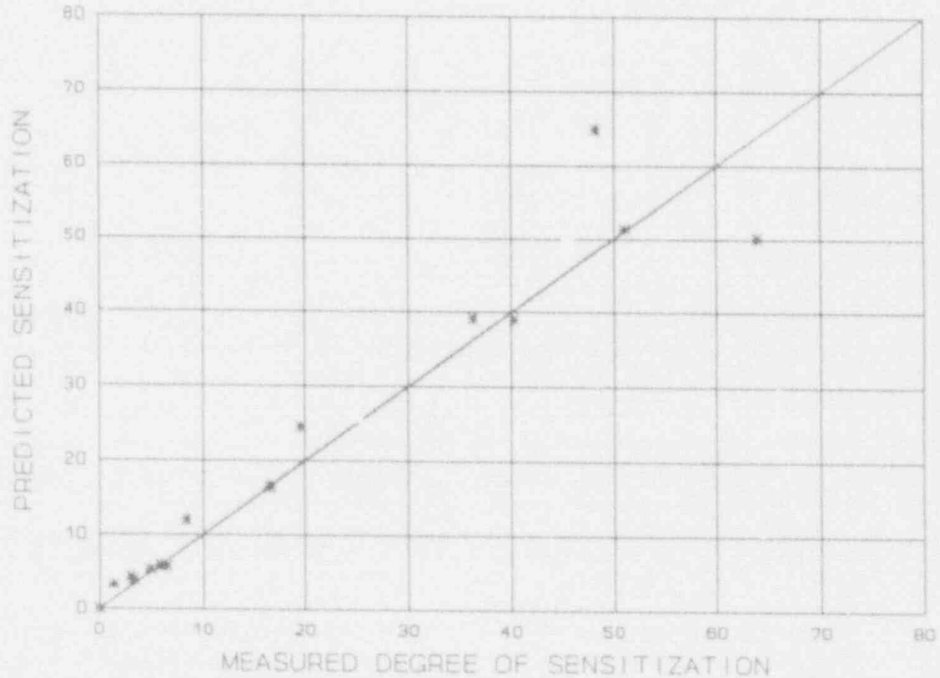

b

Figure 29. Comparison Between Measured and SSDOS-III Predicted EPR-DOS Values for Alloy 17 Material as a Function of Prestrain at a Cooling Rate of 0.05°C/sec: a) Prestrain = 10%, b) Prestrain = 20%.

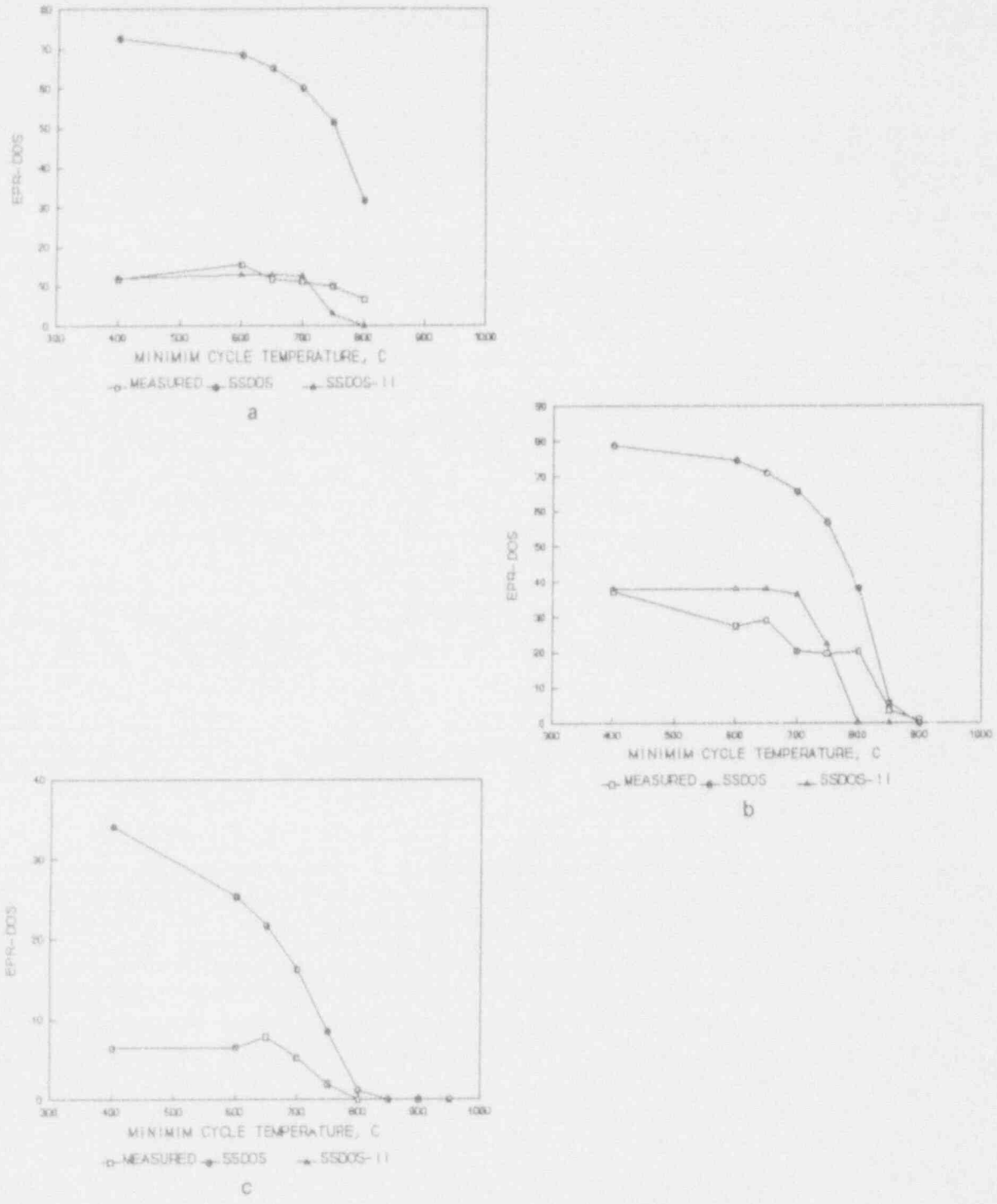

Figure 30. Comparison Between Measured and SSDOS and SSDOS-II Predicted Sensitization Development During Linear Cooling for Mill Annealed Alloy 17 as a Function of Peak Temperature at a Cooling Rate of 0.05°C/sec: a) Peak Temperature = 850°C; b) Peak Temperature = 950°C; c) Peak Temperature = 1050°C.

4.2.2 Model Application To Nitrogen Content

Another problem that arose in using the SSDOS model to predict Simmons' Gleeble data was the discrepancy between 316SS heats 16 and 17 MA materials measured and predicted EPR-DOS values.[7] Experimental results indicated that Alloy 16 exhibited greater EPR-DOS than Alloy 17 while predicted SSDOS values indicated just the opposite, Figures 32 and 33, respectively.

Assessment of SSDOS model calculations indicated that the ranking of alloys was essentially determined by their carbon content with Alloy 17 exhibiting a greater carbon content than Alloy 16, 0.067 versus 0.058 wt%C, respectively. Additional analysis of the respective alloy chemistries reveals that Alloy 17 had a considerably greater nitrogen content than Alloy 16, 0.02 versus 0.067 wt% N, respectively.

Nitrogen has been reported to compete for chromium with carbon and to subsequently be responsible for a decrease in chromium depletion rate. Thus it was postulated that the additional nitrogen in Alloy 17 was responsible for the difference in sensitization response. Subsequent SSDOS-II model modifications included an empirically driven nitrogen induced chromium depletion retardation term which resulted in Alloy 17 predictions falling below Alloy 16 predictions, see Figures 33 and 32, respectively. Complete data base assessment of the MA results for both alloy 16 and 17 indicated that SSDOS-II predictions were consistently closer than SSDOS predictions. It should be noted, however, that Bruemmer assessed his data base for possible effects of nitrogen and did not find a statistically significant effect of nitrogen[7].

4.2.3 Model Application To Initial Material Condition

Experimental results also exhibited a retardation of sensitization in SA Alloy 16 material as compared to MA Alloy 16 material, and essentially no change between SA and MA material in Alloy 17, Figures 32 versus 34 and 33 versus 35, respectively. This effect was postulated to be due to a change in grain size effect as a considerable grain size change was found in going from MA to SA material in Alloy 16 (45 to 95um, respectively) while essentially no change was found between MA and SA Alloy 17 material (60 to 75um, respectively). The SSDOS model did contain a grain size effect module but it did not seem to effect subsequent predictions for these alloys. Thus the SSDOS grain size effect on probability of initial precipitation was modified to account for measured sensitization development retardation in SA alloy 16 with respect to MA alloy 16. Subsequent SSDOS-II predictions appear to take measured grain size effects into account quite well, see Figures 32 through 35.

4.3 Model Application To Weld HAZ

The characteristics of weld thermal histories important to sensitization development are generally thought of as being the maximum temperature reached during heating and the average cooling rate during cooling. The authors propose that this is too simplified a view of sensitization development, and that, in fact, very little sensitization development occurs if one

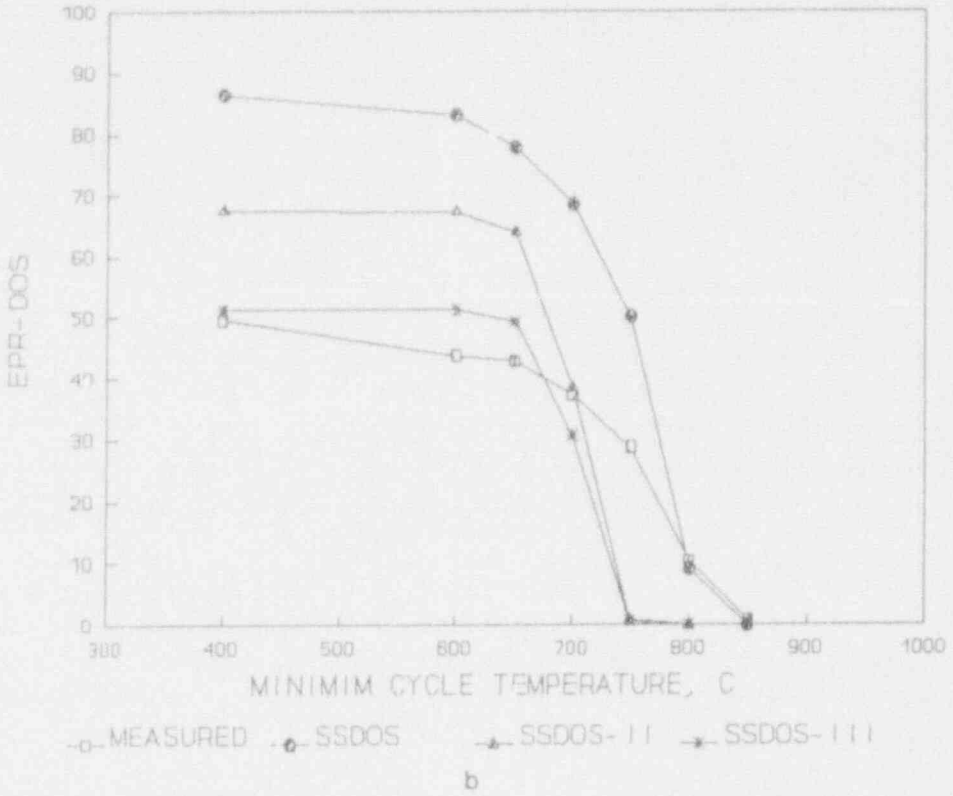

Figure 31. Comparisons Between Measured and Predicted EPR-DOS Sensitization development During Linear for Continuous Cooling for Alloy 17 prestrained 10% and cooled from a Peak Temperature of 950°C at a cooling rate of 0.05°C/sec.

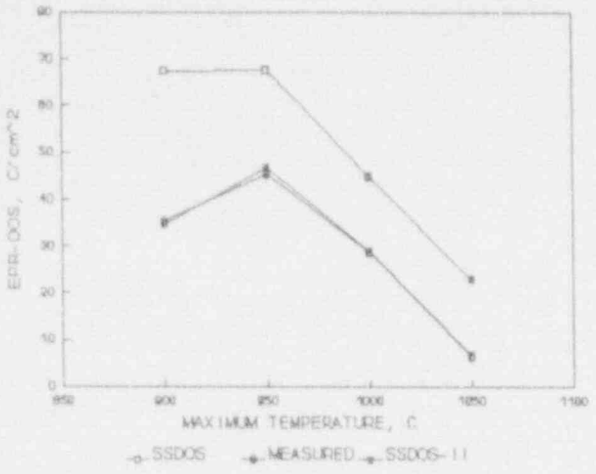

a

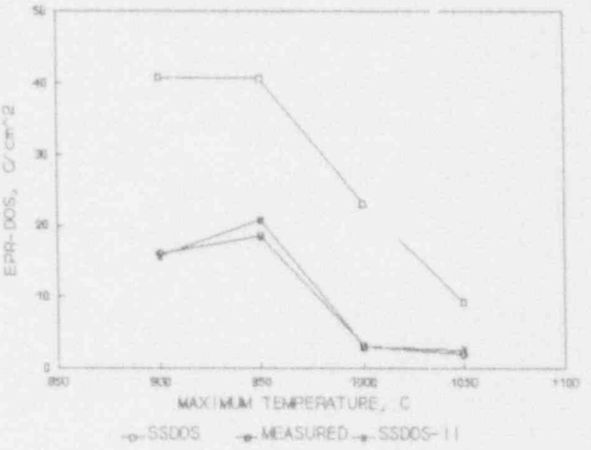

b

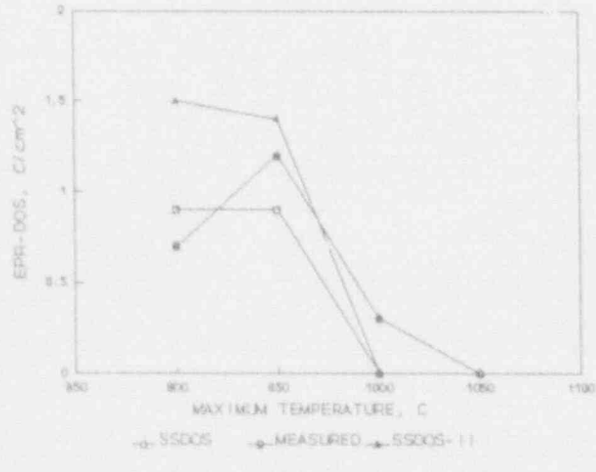

c

Figure 32. Comparison Between Measured and SSDOS and SSDOS-II Predicted EPR-DOS Values for Mill Annealed Alloy 16 Material as a Function of Peak Temperature and Cooling Rate: a) Cooling rate = 0.05°C/sec; b) Cooling rate = 0.1°C/sec; c) Cooling rate = 1°C/sec.

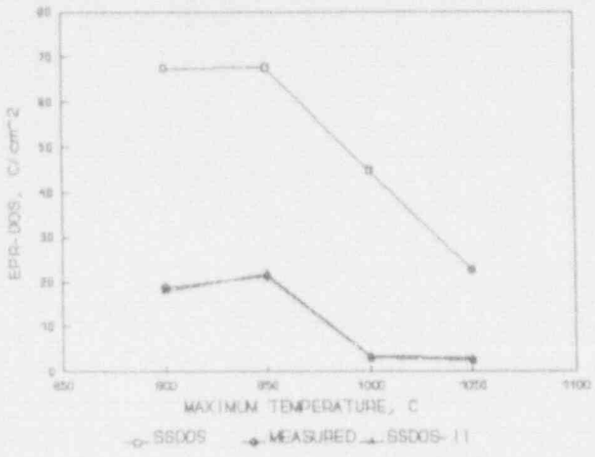

a

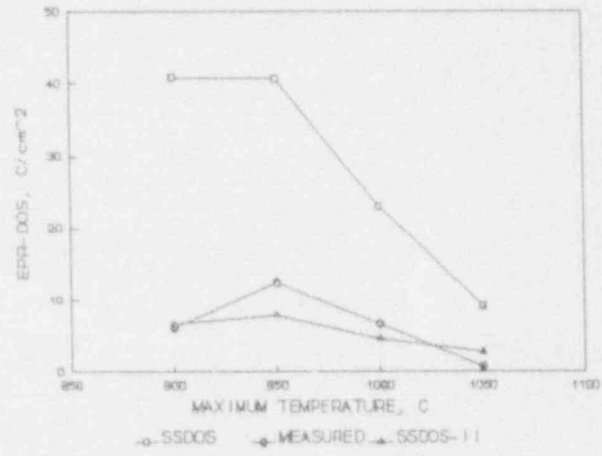

b

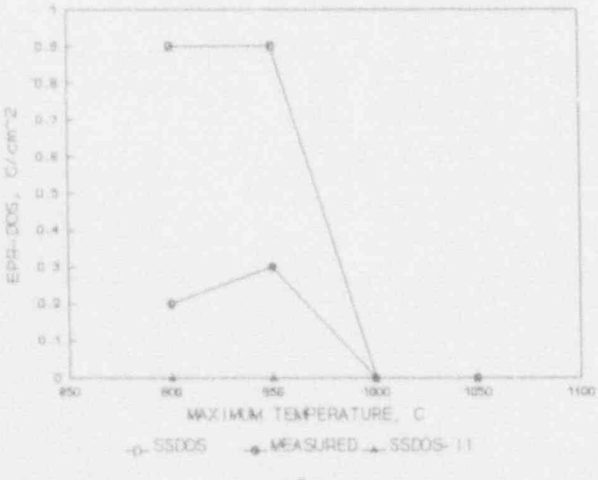

c

Figure 33. Comparison Between Measured and SSDOS and SSDOS-II Predicted EPR-DOS Values for Mill Annealed Alloy 17 Material as a Function of Peak Temperature and Cooling Rate: a) Cooling rate = 0.05°C/sec; b) Cooling rate = 0.1°C/sec; c) Cooling rate = 1°C/sec.

runs weld simulation cycles based on maximum temperature and average cooling rate. It appears that maximum sensitization development occurs in the portion of weld thermal cycle near the maximum temperature, on both the heating and cooling side, where the rate of change of temperature is smallest. Outside this region the material generally sees a relatively rapid rate of temperature change on heating and on cooling where sensitization development is relatively minimal.

An illustration of HAZ weld induced sensitization development during girth welding of a 356mm diameter, Schedule 160, 304 SS pipe is illustrated in Figure 36. The pass-by-pass, inside wall, thermal histories were experimentally measured while the chromium depletion width and EPR-DOS values were predicted using SSDOS. These predictions indicate that the majority of sensitization development, for this position with respect to the weld centerline, was associated with only two out of 16 passes, pass 6 and 7. The early passes exhibited fast heating and cooling rates as well as maximum temperatures that promoted carbide dissolution and high chromium minimums, while the latter passes didn't reach high enough temperatures to promote carbide growth.

Pass 6 had a maximum temperature near 1000°C which promoted high grain boundary chromium minimums and a decrease in chromium depletion in the region near maximum temperature. Limited increase in the size of the depleted zone took place during the relatively slow cooling cycle. The majority of the development occurred in the temperature region exhibiting a slow rate of temperature change in pass 7, i.e., near maximum temperature during heating as well as cooling. These observations demonstrate the need for "correct" simulation of the complete weld thermal cycle and the unacceptability of weld simulation using only maximum temperature and (average) cooling rate.

Another weld simulation problem that arises is the need for inclusion of deformation effects. The presence of plastic strain has been shown to accelerate both isothermal and continuous cooling induced sensitization development.[2,4,6,8] Dynamic strain measurement techniques used to monitor HAZ deformation indicates that cyclic plastic strain above and beyond that simply induced by thermal expansion is present in the HAZ.[4,28]

Deformation measuring devices, Figure 37, were placed on the inside surface of SS girth welds in order to monitor weld induced deformation. Results for twelve out of 35 passes of deformation parallel to, and 0.5cm from the weld centerline, for a 610mm diameter, 25.4mm wall, high carbon, Type 304 SS the girth weld, Figure 38, indicate a consistent pattern of deformation takes place during welding.[4,28] A proposed graphical analysis of the deformation taking place for a given pass is presented in Figure 39.[4,28] Note that the removal of thermally induced strains, based on the measured thermal history corresponding to the center of the deforming region, still leaves strain components, called "mechanical" strain, several times the magnitude of the thermal strain, Figure 39.

An analysis of mechanical strain, Figure 39, indicates that initial plastic strain is compressive, followed by a region of tensile plastic strain and then a second region of compressive plastic strain. This is then followed by a tail-off region that determines final residual (compressive or tensile) elastic strain. A detailed discussion of this analysis is given elsewhere.[28] Addition of the absolute values of strain for the three major regions results in an effective strain term on a pass-by-pass basis, as illustrated in Figure 40.

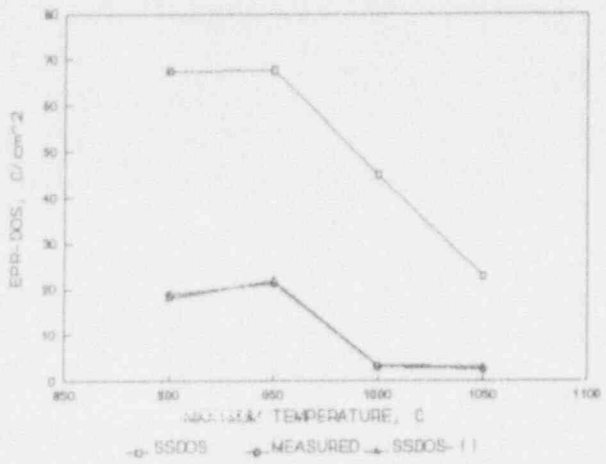

a

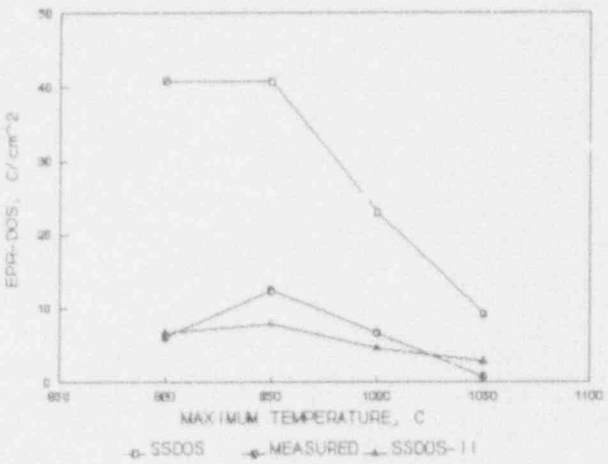

b

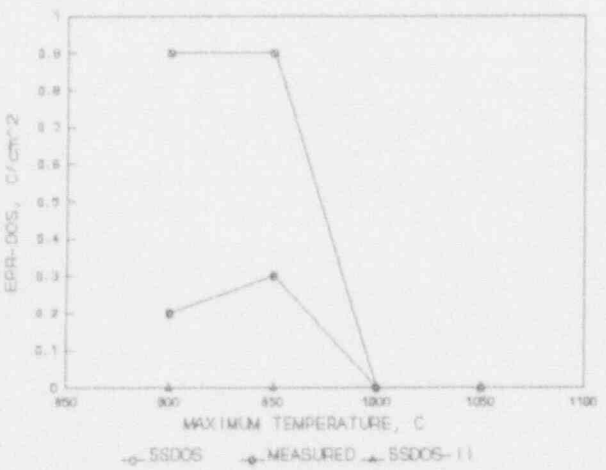

c

Figure 34. Comparison Between Measured and SSDOS and SSDOS-II Predicted EPR-DOS Values for Solution Annealed Alloy 16 Material as a Function of Peak Temperature and Cooling Rate: a) Cooling rate = 0.05°C/sec; b) Cooling rate = 0.1°C/sec; c) Cooling rate = 1°C/sec.

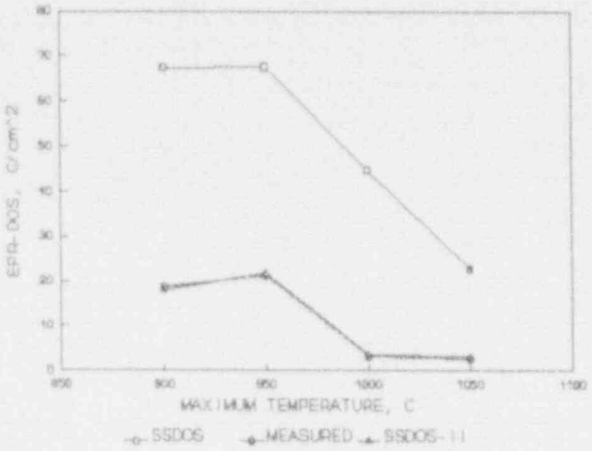

a

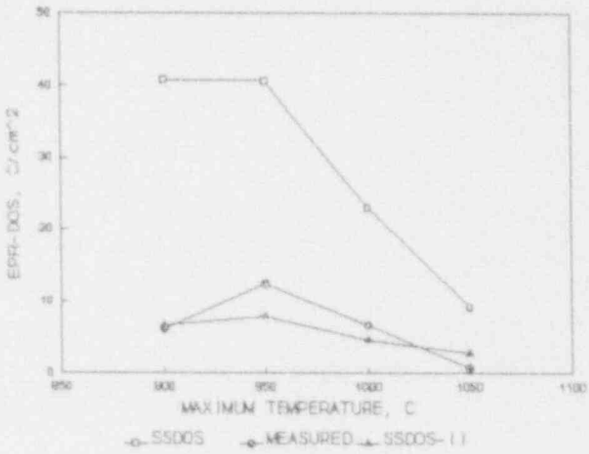

b

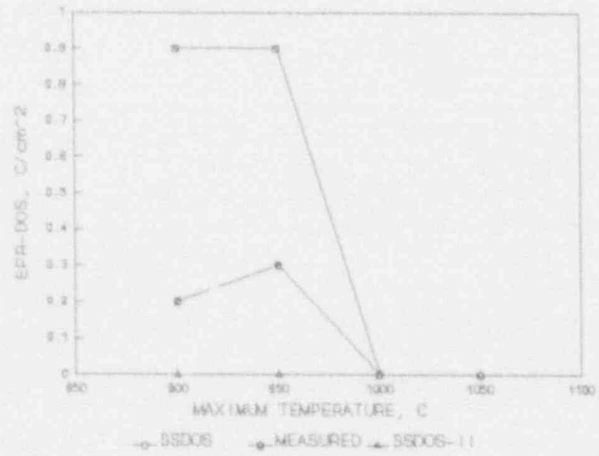

c

Figure 35. Comparison Between Measured and SSDOS and SSDOS-II Predicted EPR-DOS Values for Solution Annealed Alloy 17 Material as a Function of Peak Temperature and Cooling Rate: a) Cooling rate = 0.05°C/sec; b) Cooling rate = 0.1°C/sec; c) Cooling rate = 1°C/sec.

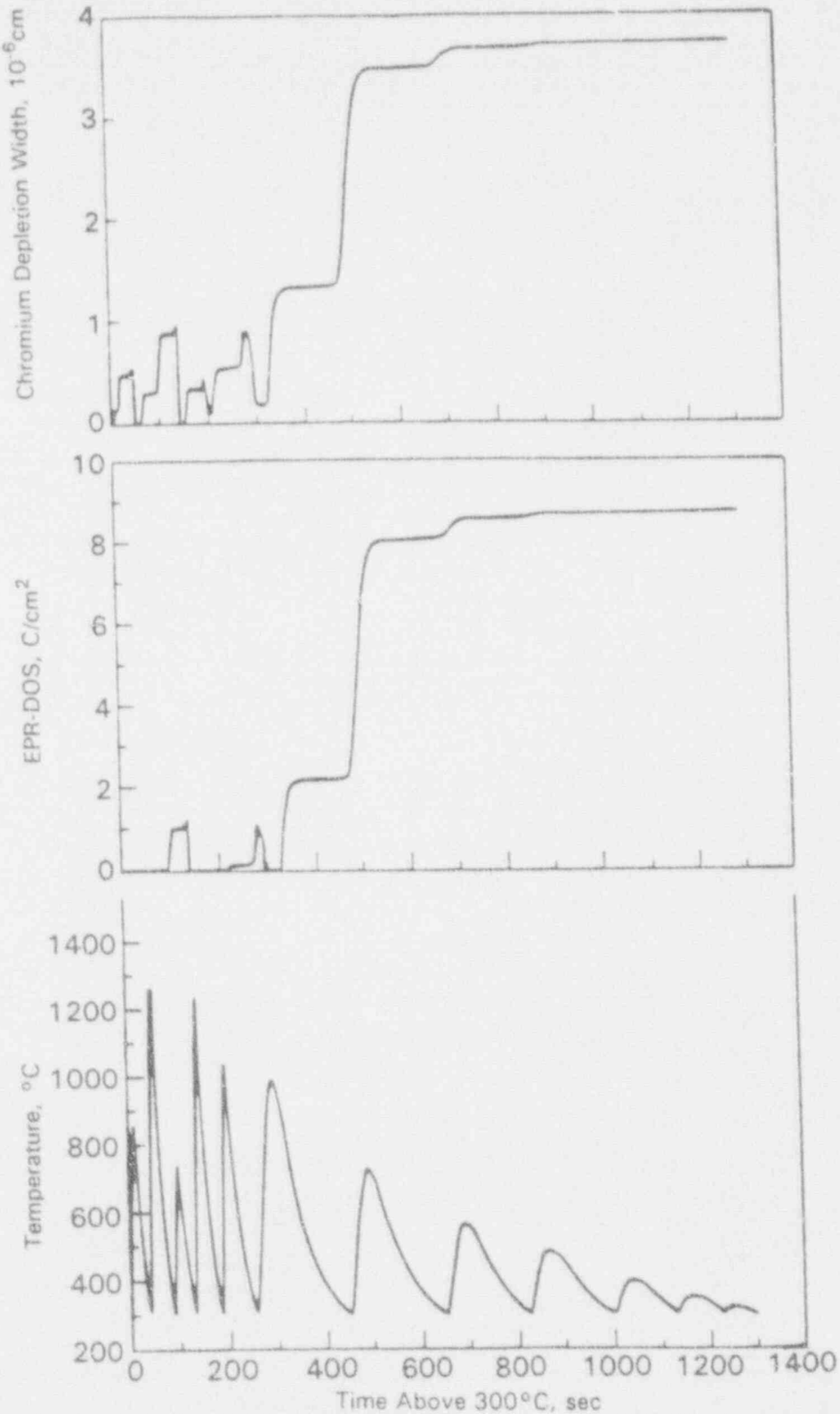

Figure 36. Development of the Degree of Sensitization 4mm from the Weld Centerline in a 356mm Diameter Schedule 160 SS Pipe Weld.

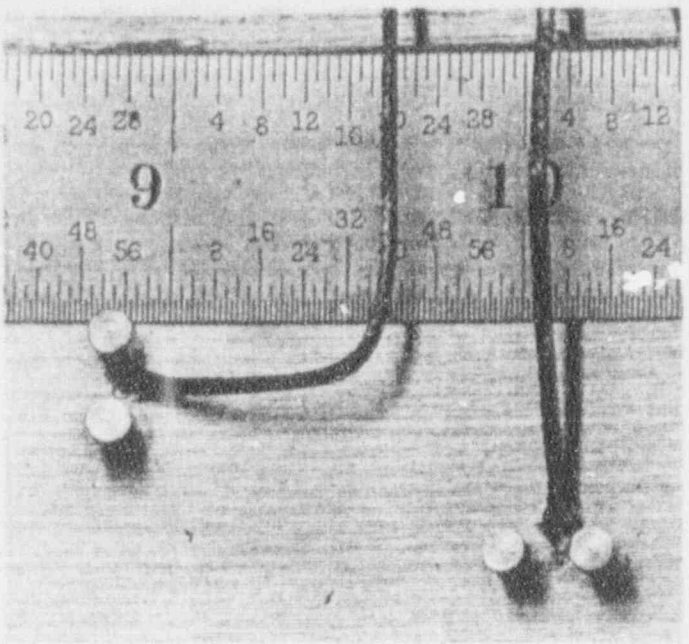

(a)

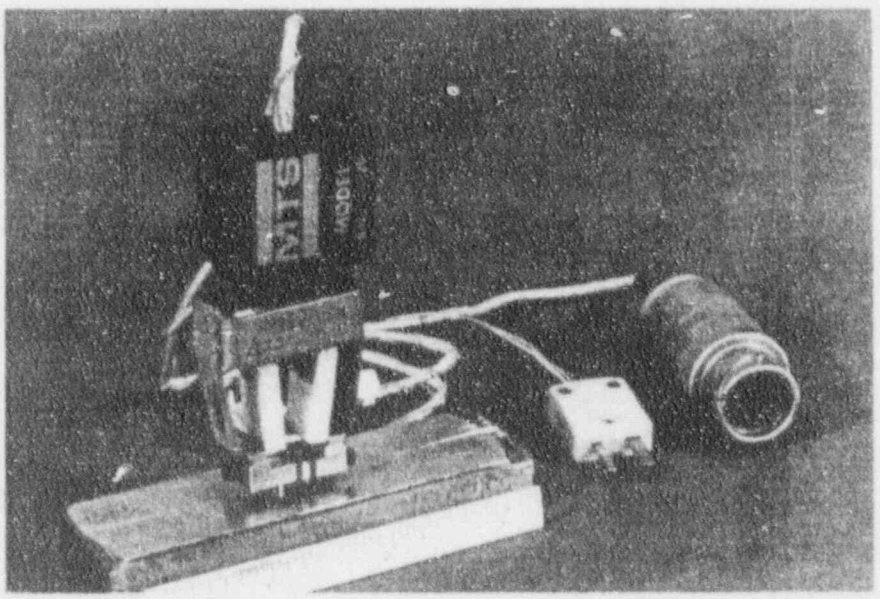

(b)

Figure 37. a) Surface Movement Monitoring Clip Gage Attachment Studs and; b) Completely Assembled Gage.

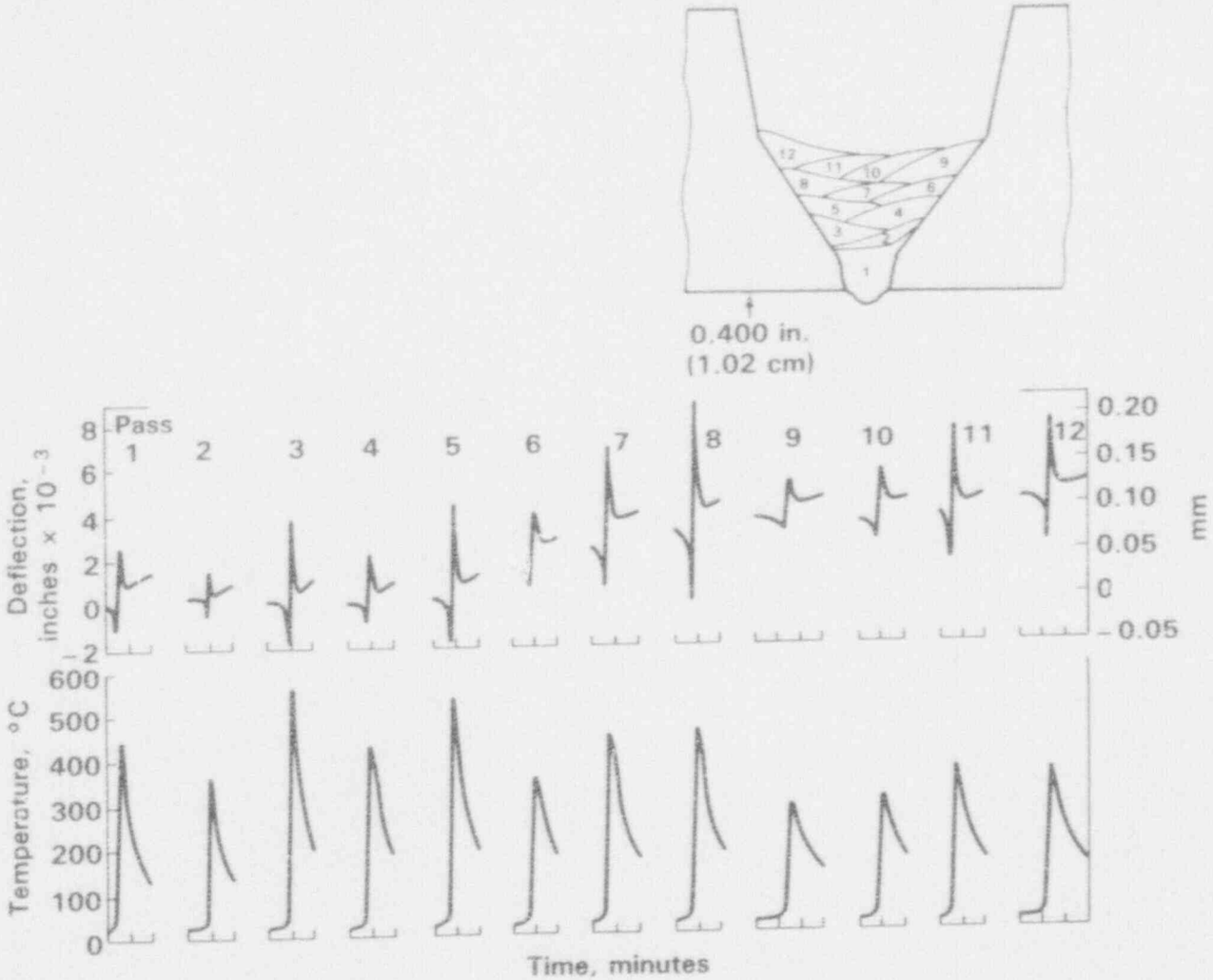

Figure 38. Temperature and Surface Deflection Parallel to the Weld Centerline Surface 10mm from the Weld Centerline for the First Twelve Passes of a 610mm Diameter Pipe Weld.

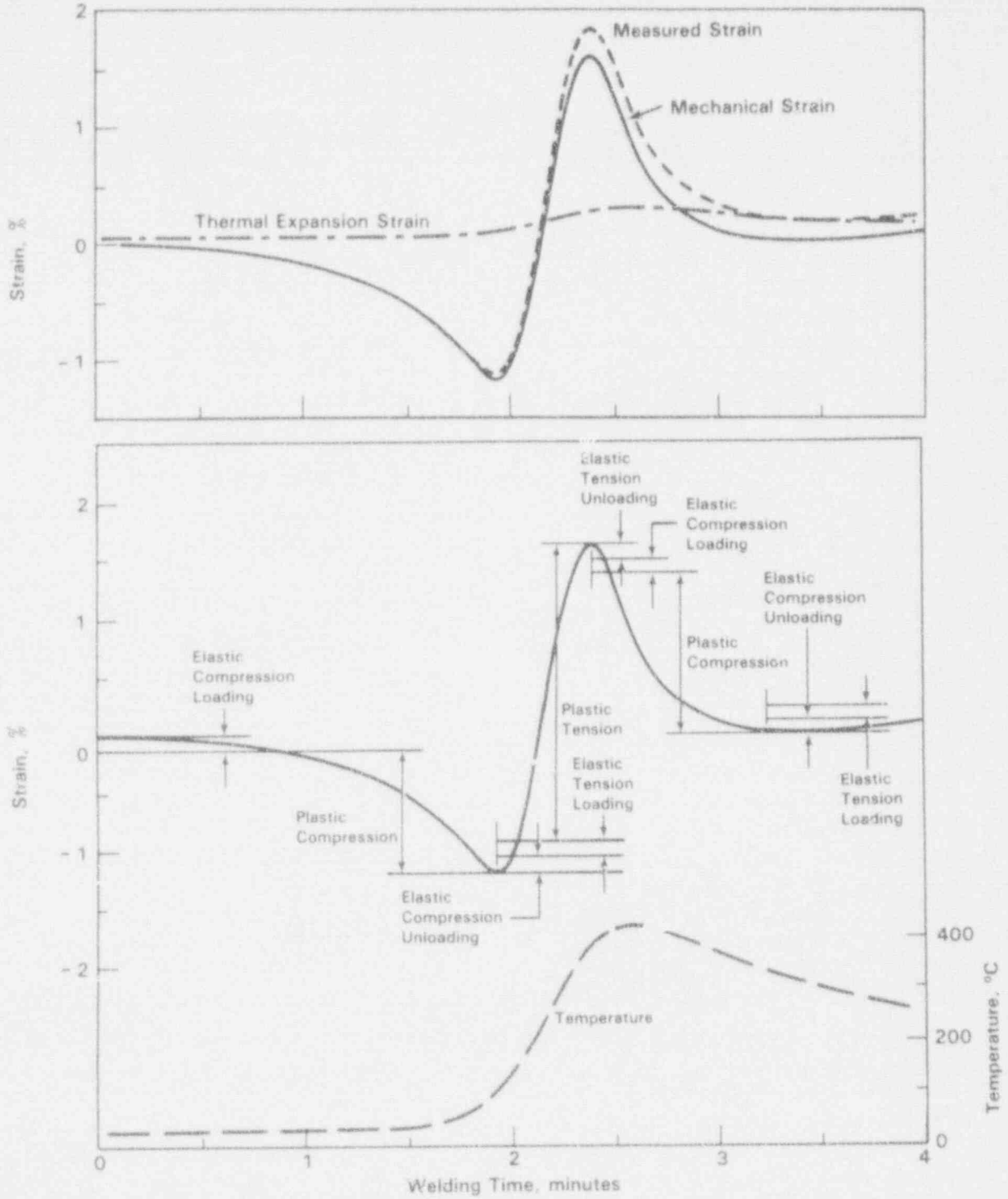

Figure 39. Thermal and Mechanical Strain Components of Stains Measured Parallel to the Weld Centerline. Data for Pass 18 at the Weld Centerline.

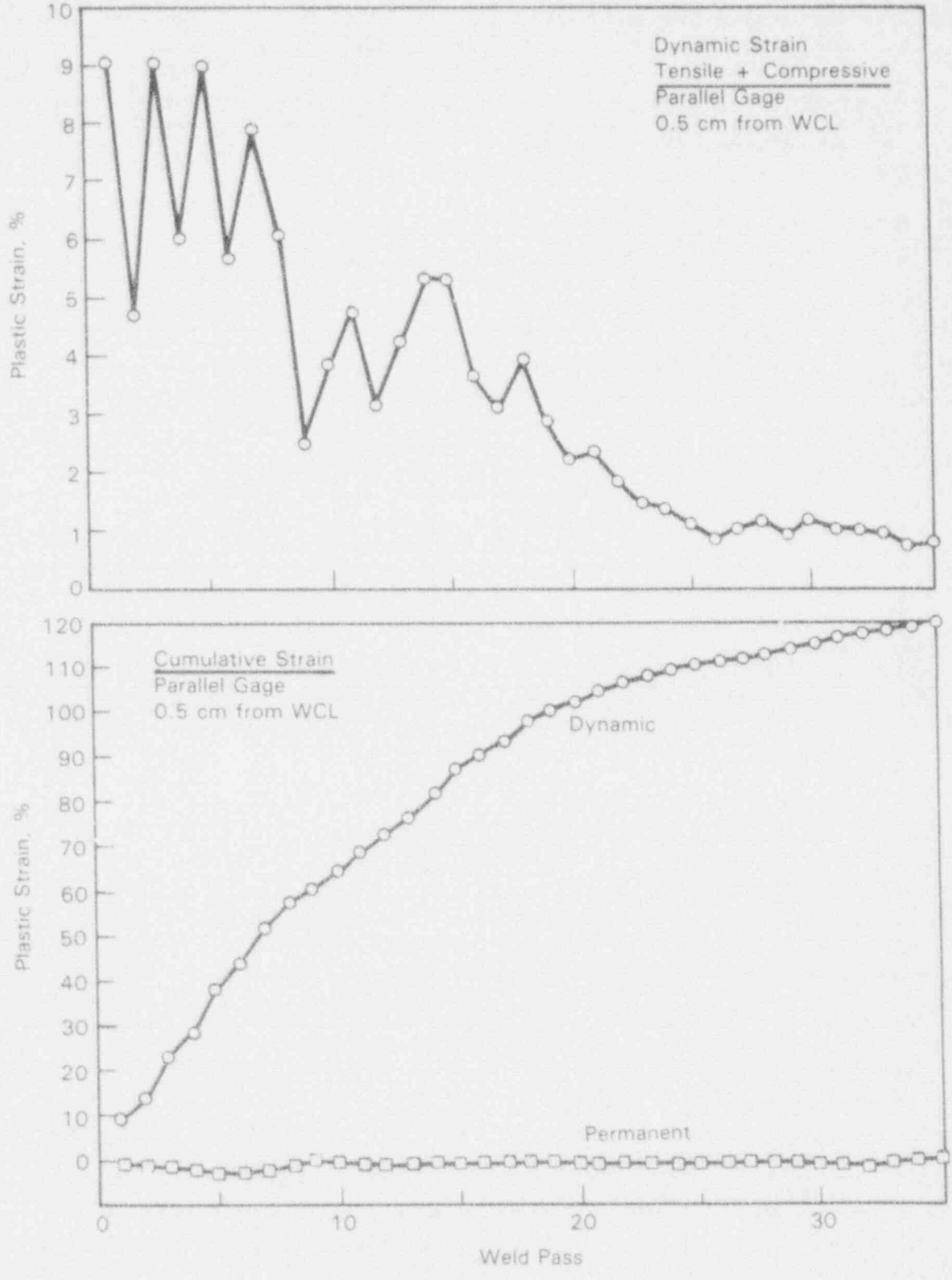

Figure 40. Pass-by-Pass and Cumulative Dynamic Strain compared to the Permanent Plastic Strain Induced at the Inner Surface 0.5mm from the Weld Centerline.

As demonstrated above, realistic weld thermal histories, including the shape of the temperature/time history instead of a simple estimate of maximum temperature and cooling rate, is required for accurate predictions. The thermal history module currently used in the model is based on the weld thermal history prediction program developed by Solomon.[29] This thermal prediction methodology yields thermal histories as a function of weld heat inputs, pipe thickness and bead placement.

The basic continuous cooling model was modified to allow input of thermal histories using Solomon's weld thermal prediction scheme. Thermal histories for a 610mm diameter, 25.3mm wall, SS pipe are shown in Figure 41. Comparison of predicted thermal histories with experimentally determined histories yielded reasonable agreement with actual maximum temperatures, Table 1. Weld heat input and bead positions for this weld simulation calculation were taken from an actual weldment and are exhibited in Figure 42.[4]

Table 1. Comparison of measured and predicted maximum temperatures on a pass-by-pass basis.

	Peak Temperature, °C	
Pass Number	Measured	Predicted
1	940	946
2	759	756
3	899	902
4	742	737
5	725	723
6	517	578

Assessment of sensitization development under multipass conditions and the effect of carbon content and strain on sensitization development in Type 304 SS is presented in Figure 43a. Three sets of sensitization development values, calculated using the thermal histories presented in Figure 41, are plotted as a function of strain level and carbon content. The first set of sensitization values assumes only thermal effects with no strain component. This is assumed to be the minimum sensitization derived from the weldment. The second set assumes base thermal effects accelerated by the measured mechanical strain induced on a pass by pass basis, Figure 40. The third set assumes thermal effects accelerated by the cumulative measured strain induced on a pass by pass basis. Use of the pass by pass measured strain assumes complete strain recovery during each weld pass. Use of the cumulative measured strain assumes no strain recovery during each weld pass. One assumes the "correct" strain values lie between the two latter extremes. Sensitization development is found to dramatically increase with increasing carbon content and strain.

Assessment of the effect of alloy content and type is presented in Figure 43b, assuming cumulative strain. Little EPR-DOS differences are found between the alloy types at low carbon concentration, with Type 316 tending to be more resistant to sensitization development at high

carbon contents than either of the two 304 alloys. The high nitrogen 304 alloy exhibits reduced sensitization in comparison to the standard 304 alloy, but greater sensitization than the standard 316 alloy. The specific Type 304 alloy composition is that of the pipe material previously girth welded is: 0.058C, 18.67Cr, 8.78Ni, 0.16Mo, and 0.059N (wt%). The post-weld EPR-DOS value found using the field cell EPR-DOS measurement technique was 28, which agrees reasonably well with the predicted EPR-DOS.[4]

Weld heat affected zones from all but the low carbon (0.02 wt%) welds would be expected to exhibit substantial reduction of area when subjected to CRT testing in simulated BWR coolant water as illustrated in Figure 1. Use of the generally accepted rule of thumb that material exhibiting between 2 to 5 EPR-DOS is susceptible to IGSCC in BWR reactor environments also indicates that only the low carbon alloys would not be susceptible to IGSCC in the as-welded conditions in BWRs not using supplemental IGSCC mitigation techniques. More quantitative predictions of IGSCC are possible by combining the EPR-DOS predictions of the SSDOS model with the model of Ford[30] which predicts crack growth rates as a function of EPR-DOS.

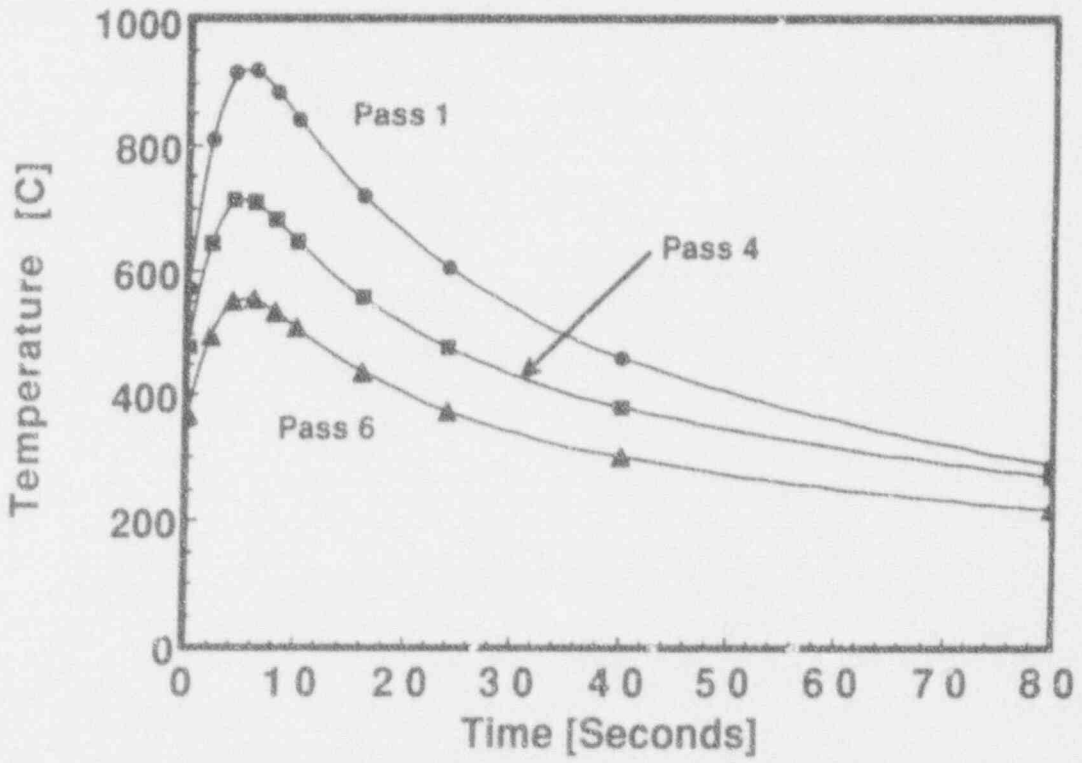

Figure 41. Predicted HAZ Girth Weld Thermal Histories 5mm from Weld Centerline on the Inside Surface of a 610mm Diameter 25.4mm Wall, Type 300, Series SS Pipe as a Function of Pass.

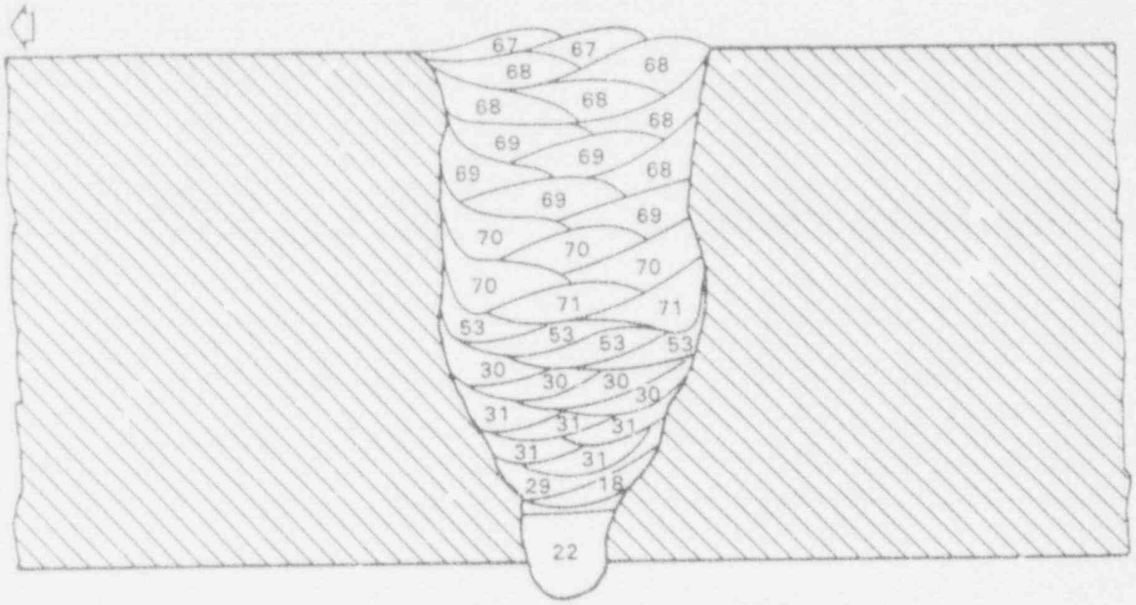

Figure 42. Schematic Illustration of Weld Bead Position and Welding Heat Input (kJ/in.) used to Girth Weld a 610mm Diameter, 25.4mm wall, Type 304 SS Pipe.

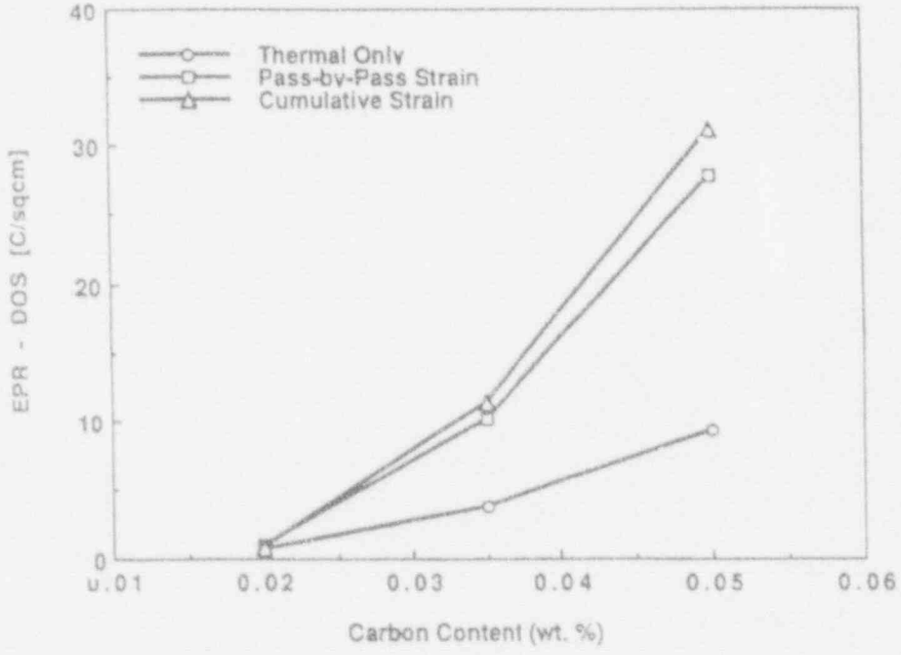

(a)

Figure 43. Predicted Post-Weld EPR-DOS 5mm from the Weld Centerline on the Inside Surface of a 610mm Diameter pipe as a function of alloy composition and local strain: a) Type 304 as a Function of Carbon Content and Thermal-Mechanical History; b) Types 304 and 316 as a Function of Carbon content Assuming Cumulative Strain Effects.

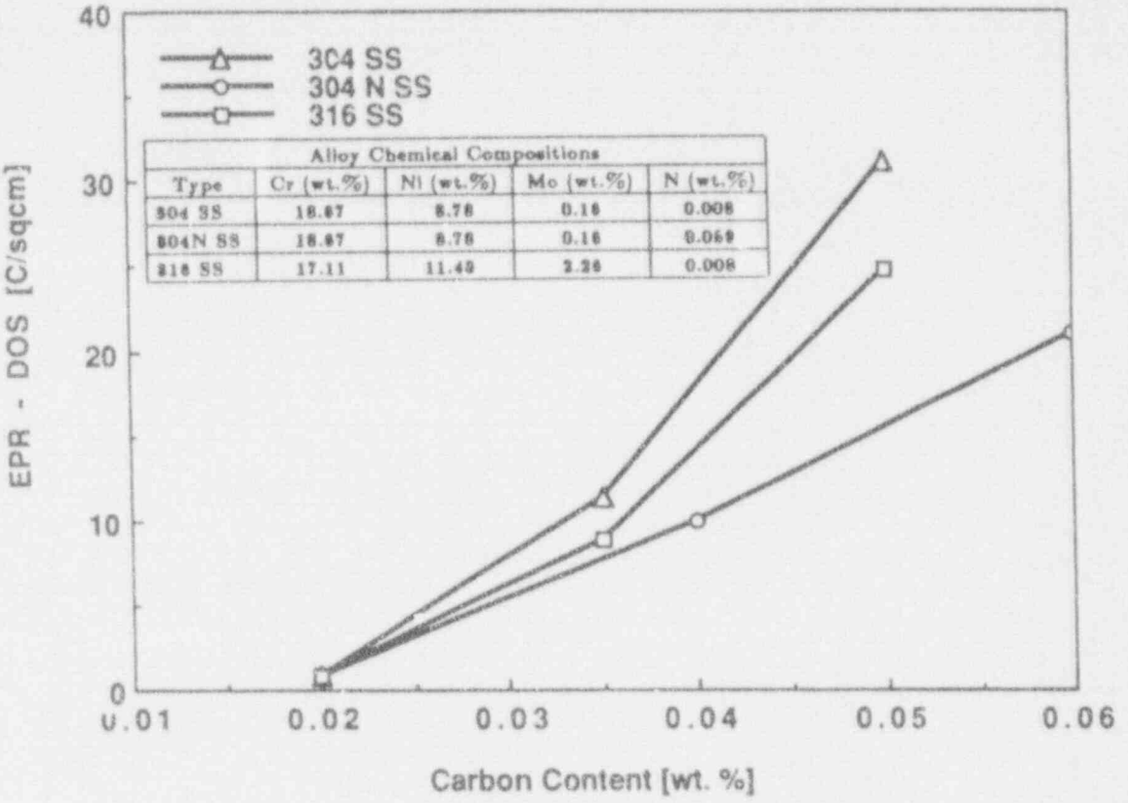

(b)

Figure 43. (Continued)

5.0 CONCLUSIONS

A computer-based model has been developed that is capable of predicting continuous cooling induced sensitization, with and without the presence of prior strain. Modeling of sensitization development kinetics required the use of nucleation time as a function of specimen temperature. Modeling of the experimentally observed decrease in sensitization development kinetics once temperatures over the solid solubility temperature of carbon was reached required a decrease in nucleation kinetics. Application of continuous cooling sensitization modeling to the welding situation proved feasible.

6.0 REFERENCES

1. E.C. Bain, R.H. Aborn and J.J.B. Rutherford, Trans. Amer. Soc. Steel Treating, 21, 481 (1933).

2. S.M. Bruemmer, "Quantitative Measurement and Modeling of Sensitization Development in Stainless Steels," Edited by D.G. Atteridge, Oregon Graduate Institute of Science & Technology, Beaverton, OR 97006-1999, U.S. Nuclear Regulatory Commission Report: NUREG/GR-0001, September (1992).

3. S.M. Bruemmer, "Quantitative Modeling of Sensitization Development in Austenitic Stainless Steel," Corrosion Journal, 146(9), 698, 1990.

4. D.G. Atteridge, S.M. Bruemmer, "Evaluation of Welded and Repair Welded Stainless Steel for LWR Service," U.S. Nuclear Regulatory Commission Report: NUREG/CR-3613, Vol. 3, No. 2, (1986).

5. D.G. Atteridge, C.A. Cedeño, "Continuous Cooling Thermal cycle Effect on Sensitization in Stainless Steels, Oregon Graduate Institute of Science and Technology, Beaverton, OR 97005-1999, U.S. Nuclear Regulatory Commission Report: NUREG/GR-002, August (1991).

6. J.W. Simmons, "Effects of Prior Deformation Continuous Cooling of Type 316 Austenitic Stainless Steel," Edited by D.G. Atteridge, Oregon Graduate Institute of Science and Technology, Beaverton, OR 97006-1999, U.S. Nuclear Regulatory Commission Report: NUREG/GR-003, August (1991).

7. J.W. Simmons, D.G. Atteridge, L.E. Murr, S.M. Bruemmer, "Effects of Prior Deformation on the Sensitization of Type 316 Austenitic Stainless Steel II: Continuous Cooling Sensitization," Recent Trends in Welding Science and Technology, Edited by S.A. David and J.M. Vitek, International Conference Proceedings, PP. 321-5, (1990).

8. A.H. Advani, "Deformation Effects on the Development of Grain Boundary Chromium Depletion (Sensitization) in Type 316 Austenitic Stainless Steels," DOE-NE-37963-12, July (1990).

9. W.L. Clarke, R.L. Cowan and W.L. Walker, in ASTM STP 656, 99 (1978).

10. W.L. Clarke, General Electric Report GEAP-21382, U.S. Nuclear Regulatory Commission NUREG-0251-1 (1976).

11. S.M. Bruemmer, L.A. Charlot, D.G. Atteridge, "Compositional Effects in the Sensitization of Austenitic Stainless Steels," U.S. Nuclear Regulatory Commission Report: NUREG/CR-3618 (1984).

12. S.M. Bruemmer, Corrosion, Vol. 42, No. 1, P. 27, January (1986).

13. J.B. Lee, Corrosion, Vol. 42, No. 1, P. 106, Febru[illegible] 986).

14. S. Pednekar, S. Smialowska, Corrosion, Vol. 36, No. 10, P. 565, (1980).[P6]

15. C.L. Briant, A.M. Ritter, Metall. Trans. Vol. 11A, P. 2009, (1980).[P7]

16. V. Cihal, "Intergranular corrosion of Steels and Alloys", Elsevier Science Publishers B.V., P. 146, (1984).[P8]

17. H.D. Solomon, D.C. Lord, Corrosion, Vol. 36, No. 8, P. 385, (1980).[P3]

18. H.D. Solomon, Corrosion, Vol. 41, No. 9, P. 512, (1985).[P5]

19. H.D. Solomon, Corrosion, Vol. 40, No. 2, P. 51, (1984).[P15]

20. M. Deighton, J. Iron Steel Inst., P. 1012, November (1973).

21. H. Ikawa, Y. Nakao, and K. Nishimoto, "Study of Weldability in SUS 304 Precipitation Phenomena of $M_{23}C_6$ During Thermal Cycles," Technical Reports of Osaka University, No. 1434, P. 363, (1978).

22. H.D. Solomon, Corrosion, Vol. 36, No. 7, P. 356, (1980.[P3]

23. C.S. Tedmon, Jr., D.A. Vermilyea, J.H. Rosolowski, J. Electrochem. Soc., Vol. 118, No. 2, P. 192, (1971).

24. C.L. Briant, E.L. Hall, corrosion, Vol. 42, No. 9, P. 523, September (1986).

25. D.G. Atteridge, S.M. Bruemmer, R.E. Page, "Evaluation and Acceptance of Welded and Repair-Welded Stainless Steel for LWR Service," U.S. Nuclear Regulatory Commission Report: NUREG/CR-3613, (1983).

26. D.G. Atteridge, S.M. Bruemmer, L.A. Charlot, R.E. Page, "Evaluation of Welded and Repair-Welded Stainless Steel for LWR Service," U.S. Nuclear Regulatory Commission Report: NUREG/CR-3613, Vol. 3, No. 1 (1985).

27. S.M. Bruemmer and L.A. Charlot, Sensitization Development in Austenitic SS: Comparison Between STEM-EDS and EPR Measurements, Corrosion Journal,44(6), 328, 1988.

28. D.G. Atteridge, W.E. Anderson, "Cyclic Work Hardening Induced in the Heat Affected Zone During Multi-Pass Welding," presented at the International Conference on Welding and Performance of Pipelines, London, England, November (1986).

29. H.D. Solomon, S. Levy, "HAZ Temperatures and Cooling Rates as Determined by a Simple Computer Program," Trends in Welding Research in the United States, PP. 173-206, Edited by S.A. David, Conference Proceedings, (1982).

30. F.P. Ford, D.F. Taylor, P.L. Anderson, and R.G. Ballinger, EPRI Report, NP50648, Feb, 1987.

NRC FORM 335 (2-89) NRCM 1102, 3201, 3202

U.S. NUCLEAR REGULATORY COMMISSION

BIBLIOGRAPHIC DATA SHEET

(See instructions on the reverse)

1. REPORT NUMBER (Assigned by NRC. Add Vol., Supp., Rev., and Addendum Numbers, if any.)

NUREG/GR-0004

2. TITLE AND SUBTITLE

Measurement and Modeling of Sensitization Development in Stainless Steels as a Function of Thermomechanical Processing

3. DATE REPORT PUBLISHED

MONTH: November YEAR: 1992

4. FIN OR GRANT NUMBER

G1107

5. AUTHOR(S)

D.G. Atteridge, S.M. Bruemmer*, J.W. Simmons, M.Li

6. TYPE OF REPORT

7. PERIOD COVERED (Inclusive Dates)

8. PERFORMING ORGANIZATION - NAME AND ADDRESS (If NRC, provide Division, Office or Region, U.S. Nuclear Regulatory Commission, and mailing address; if contractor, provide name and mailing address.)

Department of Materials Science and Engineering
Oregon Graduate Institute of Science and Technology
Beaverton, OR 97006-1999

*Pacific Northwest Laboratory
Richland, WA 99352

9. SPONSORING ORGANIZATION - NAME AND ADDRESS (If NRC, type "Same as above"; if contractor, provide NRC Division, Office or Region, U.S. Nuclear Regulatory Commission, and mailing address.)

Division of Engineering
Office of Nuclear Regulatory Research
U.S. Nuclear Regulatory Commission
Washington, DC 20555

10. SUPPLEMENTARY NOTES

11. ABSTRACT (200 words or less)

An analytical model has been developed for predicting thermomechanical effects on the development of grain boundary chromium depletion in austenitic stainless steel as a first step in predicting intergranular stress corrosion cracking susceptibility. Model development and validation is based on sensitization development analysis of over 30 Type 316 and 304 stainless steel heats. The data base included analysis of deformation effects on resultant sensitization development. Continuous cooling sensitization behavior is examined and modeled with and without strain. Gas tungsten arc girth pipe weldments are also characterized by experimental measurements of heat affected zone temperatures, strains and sensitization during/after each pass; pass by pass thermal histories are also predicted. The model is then used to assess pipe chemistry changes on chromium depletion changes.

12. KEY WORDS/DESCRIPTORS (List words or phrases that will assist researchers in locating the report.)

austenitic stainless steel, sensitization, welding, chromium depletion, modeling, continuous cooling, strain effects

13. AVAILABILITY STATEMENT

Unlimited

14. SECURITY CLASSIFICATION

(This Page) Unclassified

(This Report) Unclassified

15. NUMBER OF PAGES

16. PRICE

Federal Recycling Program

UNITED STATES
NUCLEAR REGULATORY COMMISSION
WASHINGTON, D.C. 20555-0001

OFFICIAL BUSINESS
PENALTY FOR PRIVATE USE, $300

FIRST CLASS MAIL
POSTAGE AND FEES PAID
USNRC
PERMIT NO. G-67

120555139531 1 1AN1R5
US NRC-OARM
DIV FOIA & PUBLICATIONS SVCS
TPS-PDR-NUREG
P-211
WASHINGTON DC 20555